AIAA/CEAS 98-2261

Acoustics and Aeroperformance of Nozzles with Screwdriver Shaped and Axisymmetric Plugs

M. Gilinsky
Hampton University, Hampton, VA, USA

V.M. Kouznetsov
Central Aerohydrodynamics Institute
(TsAGI), Moscow, Russia

and

D.M. Nark
Hampton University, Hampton, VA, USA

4th AIAA/CEAS Aeroacoustics Conference
June 2-4, 1998 / Toulouse, France

ACOUSTICS AND AEROPERFORMANCE OF NOZZLES WITH SCREWDRIVER SHAPED AND AXISYMMETRIC PLUGS

Mikhail Gilinsky†
Hampton University, Hampton, Virginia 23668
Vladimir M. Kouznetsov‡
Central AeroHydrodynamics Institute (TsAGI), Moscow
and
Douglas M. Nark*
Hampton University, Hampton, Virginia 23668

Abstract

The recent experimental and numerical tests of corrugated nozzles have shown some acoustic and thrust benefits relative to traditional round nozzles [1 – 3]. For example, a Bluebell nozzle which was obtained by 3D nozzle design incorporating a corrugated cross section nozzle shape with a sinusoidal lip line nozzle edge, can provide an acoustic benefit up to 4dB with ~1% thrust augmentation. In references [1 – 3], this effect was explained as being the result of the corrugated design producing more efficient mixing of the exhausted jet with ambient air. Based on this argument, the authors [4] have proposed the application of this concept for a centerbody (plug) which can form several vortices downstream from the centerbody.

Several different corrugated designs are proposed and described in detail in this paper. The main design is a Screwdriver shaped centerbody or plug (SCR) which was tested experimentally and numerically. The acoustic tests were conducted in the anechoic chamber of the Central AeroHydrodynamics Institute (TsAGI, Moscow) under Civilian Research and Development Foundation (CRDF) grant. These experiments have shown an essential acoustic benefit of ~10-13% with the application of the co-annular nozzles by comparison with the reference round nozzle with the same mass flow rate. However, the expected acoustic benefits with the application of the 4-petal Screwdriver shaped centerbody were not obtained by comparison with the reference axisymmetric centerbody (CON) having the same length and the same cross section areas at the same distance from the nozzle throat. Moreover, for some angles ($\theta = 60°$ amd $90°$) noise increase was observed (~1-3%). These tests will be continued with the goal of obtaining better acoustic results. In particular, acoustic characteristics are hoped to be improved by moving the centerbody into the nozzle and using penetrable walls for the SCR and/or for the main nozzle. Preliminary results for such approach are very promising.

Aeroperformance effects were analyzed numerically. The nozzle thrust calculations were based on a full Navier-Stokes equations solver (NSE), and both full and marching Euler codes: CFL3D [7], CRAFT [8], and Krayko-Godunov [9]. Grid preparation and its optimization were conducted using GRIDGEN and our own codes. The general conclusion of this numerical analysis is some thrust loss with the application of SCR design (~1-1.5%). But, again, some constructive features of SCR design give some promising perspectives for its application in aviation and domestic industries.

1. A Screwdriver centerbody (plug) geometry

A Screwdriver body shape was discussed many years ago in connection with an application of such a configurations as the front part of bullets, projectiles and rockets. This shape provided lower drag and higher stability of forward flight for rotating projectiles. These surfaces belong to a family of shapes formed out of by rectilinear intervals joining corresponding points of two different closed curves in space. A Screwdriver body uses a circle as an initial curve and one or several crossing rectilinear intervals as an end curve. Usually, these intervals are symmetrically located relative to a body's axis of symmetry. In subsequent discussion, several different modifications of Screwdriver shaped centerbody surfaces will be described.

1.1 Rectilinear Screwdriver Shaped Surfaces. We use a cruciate Screwdriver shaped centerbody. A 4-petal Screwdriver centerbody is shown in Figure 1a. Here a convergent nozzle **1** contains a cylindrical centerbody and downstream, after the throat, it transfers to a Screwdriver centerbody. The front view from downstream is shown in Figure 1b. There are several geometric parameters which define the centerbody: number of petals, petal size and centerbody length. The axisymmetric centerbody with conical or optimal contour in a meridional plane can be taken as a baseline centerbody for comparison and for definition of Screwdriver centerbody efficiency. Figure 2 demonstrates four different modifications of Screwdriver centerbodies based on the conical centerbody. These shapes correspond to a baseline conical centerbody (**a**), and 2(**b**),3(**c**),4(**d**) and 6-petal (**e**) centerbodies. The surface sketch, coordinate system, nomenclature and surface equation for a region between two planes of symmetry are illustrated in Figure 2f. These surfaces are

† Research Professor, Senior Member AIAA
‡ Professor, TsAGI Acoustic Division Chief
* Research Assistant, D.Sc.

formed as follows. The 45°-arc of the cylindrical portion and vertical interval x_e, z_e^o are divided by I subintervals $[a_i, a_{i+1}]$ and $[b_i, b_{i+1}]$ respectively, where i=0,1,2,...I. Then, the corresponding points a_i and b_i are joined by rectilinear intervals and these intervals form the needed surface.

Our hypothesis is as follows. For example, in the case of a 4-petal centerbody, four symmetrical flow regions occur between two neighboring petals. Three-dimensional flows form downstream with swirls at the local symmetry line as shown in Figure 1a. These four anti-symmetric swirls meet each other after this point at some angle and form large vorticities downstream. Schematically such swirl flows are illustrated in Figure 1a. This enhances mixing of the jet exhaust with ambient air and can result in jet noise reduction. This 3D centerbody shape also favors flow stagnation at the local symmetry line which increases pressure on the lateral surface of the centerbody. For the same reason, such a 3D flow produces a thinner boundary layer than the usual axisymmetric flow. As a result we can expect the minimal thrust loss and in some cases even thrust augmentation through a Screwdriver centerbody application by comparison with a baseline conical centerbody. However, the final conclusion can be drawn only after additional theoretical research, numerical simulation and experimental tests.

1.2 Longitudinal Curvilinear Screwdriver-Shaped Surfaces. The second option may be more promising for designing a Screwdriver centerbody. It can help to avoid possible formation of separation zones and internal shock waves immediately downstream of the throat. This approach serves to smooth the transonic nozzle wall and the sharp wall regions at the symmetry planes. Only two simple method of such smoothness will be shown. In the case shown in Figure 2f, longitudinal rectilinear lines are replaced by curvilinear lines so that they are a smooth continuation of corresponding straight lines on a cylindric portion having a horizontal tangent at the end of a centerbody, i.e. at the rectilinear ending interval $x_e z_e^o$ in Figure 2f. Thus, these curves should have points of inflection so that they may be given by the two power functions with conjugation at these points of inflection. In the simplest case, these functions can be written as follows. Let an initial point a_i and ending point b_i have Cartesian coordinates $x_o^o = 0$, $y_o^o = r_o cos(\phi_i)$, $z_o^o = r_o sin(\phi_i)$, where r_o is the cylindrical portion radius and ϕ_i is the polar coordinate of the initial point. For uniform splitting, $\phi = (i/I)\pi/4$, $z_e = z_e^o(1 - i/I)$. The curve joining these points can be described in Cartesian variables as:

$$z(\xi) = z_o - a_z \xi^{p_1}, \qquad y(\xi) = y_o + a_y \xi^{p_2} \quad if\ 0 \le \xi \le \xi_c \tag{1.1}$$

$$z(\xi) = z_e + b_z(1-\xi)^{q_1}, \quad y(\xi) = b_y(1-\xi)^{q_2} \quad if\ \xi_c \le \xi \le 1 \tag{1.2}$$

where p_1, q_1, p_2, q_2 are fixed even powers, and ξ_c is a fixed conjunction coordinate of the two power functions which can be varied. The coefficients a_z, b_z, a_y, b_y are defined from the conjunction conditions: equality of the function and its first derivatives so that, for example, for $p_1 = p_2 = p$ and $q_1 = q_2 = q$ these coefficient are:

$$a_z = \frac{q f(\xi_c)}{\xi_c^{p-1}}, \quad b_z = -\frac{p f(\xi_c)}{(1-\xi_c)^{q-1}}$$

$$f(\xi_c) = \frac{(z_o - z_e)}{q\xi_c - p(1-\xi_c)}. \tag{1.3}$$

Several different views of such designed sonic nozzles with the 4-petal Scredriver centerbody are shown in Figure 3a-e. The equivalent (with equal cross section area) axisymmetric centerbody is in Figure 3f. These nozzles were designed and drawn at NASA LaRC and then manufactured and tested at TsAGI, Moscow in Russia. The results will be discussed below in the 2nd section .

1.3 Bluebell Screwdriver Shaped Surfaces. The third possible configuration of a Screwdriver type centerbody is based on the Bluebell nozzle concept. Let the cross section of a Bluebell shaped design decrease, instead of increase as in a divergent conical design. In this case, the cross sectional area of the baseline round conical centerbody decreases from the maximal value at the throat to zero at the axis of symmetry. As before, we require equality of both areas but increase the corrugation amplitude, for example, linearly from the throat to the end. Then we will form a smooth surface with "cavities" and "convexities" like a Screwdriver centerbody. For example, the cross sectional contour of the centerbody may be produced by using the same power functions as in the previous case for longitudinal lines (1.1-1.3). The normalized variable ξ may be replaced by a normalized variable $\eta = \phi/\phi_{max}$, where ϕ is an angle cylindric coordinate and ϕ_{max} is a half-period of symmetry of a full cross section contour function, which for a 4-petal Screwdriver is equal $\pi/4$. Thus, the dependence of the radial cylindric coordinate r on the normalized polar coordinate η is:

$$r(\eta) = r_+ - a\eta^p, \quad if\ 0 \le \eta \le \eta_c \tag{1.4}$$

$$r(\eta) = r_- + b(1-\eta)^q, \quad if\ \eta_c \le \eta \le 1. \tag{1.5}$$

Here again, η_c is a conjunction point; $r_+(x)$ and $r_-(x)$ are maximal and minimal radial coordinates in the cross section x=const; p and q are fixed power parameters; and the coefficients a and b are defined from conjunction conditions, so that:

$$a = qg(\eta_c)/\eta_c^{p-1}, \quad b = pg(\eta_c)/(1-\eta_c)^{q-1}.$$

$$g(\eta_c) = (r_+ - r_-)/[q\eta_c + p(1-\eta_c)]. \quad (1.6)$$

In the particular case when a middle point of an interval $0 \le \phi \le \phi_{max} = \pi/n_\phi$ coincides with a point of inflection, it is simpler to use the Cosine function instead of equations (1.4, 1.5):

$$r(\phi) = \frac{r_+ + r_-}{2} + \frac{r_+ - r_-}{2} cos(n_\phi \phi), \quad 0 \le \phi \le \pi/n_\phi \quad (1.7)$$

Further Screwdriver shaped centrbodies may be designed with more complex shapes which would promote the production of vorticity, thereby enhancing mixing. For example, if a straight line edge is replace by an arc shape interval, designs such as those seen in figure 4a,b may be produced. The design in figure 4a incorporates petals which are located symmetrically about the longitudinal axis. It would be expected that this geometry would not lend a great deal to the production of vorticity. Figure 4b shows a design constructed with adjacent petals located anti-symmetrically about the longitudinal axis. This would be expected to produce angular momentum, which may be useful in some application in which several nozzles are involved. Rotation of the centerbody may be included to further enhance mixing, reduce noise, and augment thrust for this and other Screwdriver designs.

1.4 Chisel Shaped Centerbody. A Chisel shaped centerbody is a modification of a Bluebell shaped centerbody and its cross section contour is described by a periodic piecewise smooth function. Detailed consideration of such functions applicable for Chisel nozzles are in reference [1]. Two examples of such centerbodies and corresponding cross section contours are shown in Figures 5a-d for 8 and 4-petal designs respectively. The general idea of this design is to favor a gradual formation of a swirl flow downstream with minimal thrust loss, and possibly in some cases, with thrust augmentation. Wing aerodynamic theory helps to construct such a three-dimensional centerbody. A gas flowing along a vertical wall produces a larger thrust if corrugation convexities are contracted to the centerbody end (as in the case of an aerofoil or a diamond-shaped wing). For the simplest design in Figure 5, dependence of radius on the azimuthal angle in the cross section is described by a periodic function $r = r(\varphi)$ with a period T=$2\pi/n_c$: into the first period $r = r_+$=const for $0 \le \varphi \le \varphi_1$ and $\varphi_2 \le \varphi \le T$, and $r = r_-$=const for $\varphi_1 \le \varphi \le \varphi_2$, where $\varphi_1 = 0.5(T - \Delta\varphi)$ and $\varphi_2 = 0.5(T + \Delta\varphi)$. We call a corrugated surface part a "cavity" or a "convexity" relative to an internal normal to the nozzle wall . A cavity depth (or a convexity height) defined by the equality $\Delta r = r_+ - r_-$, increases along the nozzle centerline from zero at the initial cross section, $x = x_o$, to the maximum value at the exit $\Delta r = \Delta_e r\xi$, where $\xi = (x - x_o)/(x_e - x_o)$, i.e. this coincides with the definition of a corrugation amplitude coefficient δ. A cavity (convexity) width, $\Delta\varphi = \varphi_2 - \varphi_1$, also linearly increases (decreases) downstream from zero (maximum) at the initial section to the maximum (zero) at the nozzle exit, i.e. $2\varphi_1 = T - \Delta\varphi = T\xi$. If nonlinear functions $r_+(x), r_-(x)$ equal zero at the ends of the interval $0 \le x_o \le x_e = 0$, the centerbody has a shape as seen in Figure 5 (for parabolic dependence). If only $r_-(x)$ satisfies these conditions, and $r_+(x_e)$ is not zero, a Screwdriver centerbody is formed. Note that these piecewise smooth contours are limited cases of the smooth contours described in the section 1.1.3 if power coefficients p and q in equations (1.4,1.5) limit to infinity.

For such a configuration two expanded flows near the nozzle wall flow into two neighboring cavities to meet each other at some angle α, mutually penetrate and more effectively mix. A flow impulse on the lateral area of the convexities increases the resulting nozzle thrust.

1.5 2D Screwdriver Shaped Surfaces. We expect to obtain similar effects in the case of a 2D nozzle through the application of linear surfaces. Such a nozzle is a 2D analogue of an axisymmetric Screwdriver centerbody. An individual element of such a construction is shown in Figure 6a. The nozzle contains a rectangular throat. A 2D plug is made with straight lines, which join points on the throat horizontal side with the vertical interval at the nozzle (or plug) edge. Such elements can be multiply repeated and form a cellular nozzle. An example of a two-cellular nozzle is shown in Figure 6b. As in the previous case of an axisymmetric flow, two anti-symmetric swirls form at the lower straight lines of two neighboring "ravines". These ravines meet each other at the edge on the vertical interval. Two crossing swirl flows create large vorticity downstream. Schematically, such swirl flows are illustrated in Figure 6c. The surface geometry and the surface equations are shown in Figure 6d.

The proposals described in this paragraph are only preliminary observations, based on the approximate estimations, on our experience, and some numerical simulations. Determination of Screwdriver shape efficiency can be drawn only after detailed theoretical research, numerical simulation, and experimental tests.

II. Acoustic Tests of Screwdriver Shaped and Axisymmetric Centerbodies (Plugs)

For examination of the described above concept, several experimental and numerical tests were conducted. Acoustic tests were made in the anechoic chamber of the Central AeroHydrodynamics Institute (TsAGI, Moscow) [5,6]. The interior dimensions of the facility within the wedged tips are 9.6x5.3x4.2m high. Three nozzle designs with exhaust jets were tested. All designs had axisymmetric external nozzles with a design exhaust Mach number M_e=1.5 and three different internal

parts: **a)** the coaxial 4-petal Screwdriver shaped centerbody/plug (SCR), **b)** the coaxial axisymmetric plug with the length and cross sections equal to the Screwdriver shaped plug (CON), and **c)** the reference round nozzle (REF) without a plug with a mass flow rate equal to that of the previous co-annular nozzles. The two photos of the first designs, **a)** and **b)**, are shown in Fig.7, and the meridional plane view with the main sizes for the CON design are in Fig.8.

The nozzle pressure ratio (NPR) is varied in the interval π_c=1.6-4.5 with a cold, supersonic, and underexpended exhaust jet. The measurement procedure in the anechoic chamber and the method of automatic data processing are illustrated in Fig.9. Microphones (model 4136/Brul&K'err Co) with cathodic recapitulators (model 4633) are established on the meridonal plane at the circular arc with the radius $R_m = 2m$ with different observation angles θ to a positive (downstream) jet axis into an interval $30^o \leq \theta \leq 105^o$. Microphone signals are transmitted to the magnetic recorder "Sony KS-616U" through an amplifier (model 2608). Decoding of acoustic pressure pulsations was conducted by an analyzer (model 2032/Brul'&K'err Co.) and PC-286 computer which provided a narrow band spectrum with a band size $\sim \Delta f$=32Hz. A Pentium computer was used for transformation of narrow band spectrums to 1/3-octave spectrums.

These experiments have shown an essential acoustic benefit ~10-13% with the application of the co-annular nozzles by comparison with the reference round nozzle. In Fig.10 narrow band spectra of jets issuing from the three supersonic nozzles are compared with the the same mass flow rate and with the nozzle pressure ratios, NPR=1.6, 1.8, 2.0, 2.4, 3.0, and 3.5. Results for the round nozzle without a centerbody (REF) are shown by black lines, the nozzle with the axisymmetric centerbody (CON) by red line, and the nozzle with the Screwdriver shaped centerbody (SCR) by blue lines. Here the observation angle is $\Theta = 30^o$.

The expected acoustic benefits of the Screwdriver shaped plug application were not obtained by comparison with an axisymmetric plug. Moreover, for some angles ($\theta = 90^o$), a noise increase was observed (~1-2%). In Fig.11, narrow band spectra of jets issuing from the two supersonic nozzles with the same mass flow rate; nozzle pressure ratios, NPR=1.6, 2.4, 3.5, and 4.5; and three observation angles, $\theta = 30^o, 60^o$, and 90^o are compared. Results for the CON design are shown by blue lines and results for the SCR design by yellow lines. 1/3-octave band spectra for the previous nozzle pressure ratios, and the four observation angles $\theta = 30^o, 45^o, 60^o$, and 90^o are in Fig.12. Results for the CON design are designated by blue lines and results for the SCR design by yellow lines. Influence of the azimuthal angle Φ on narrow band spectra at the three observation angles, $\Theta = 30^o, 60^o$, and 90^o, the three azimuthal angles, $\Phi = 0^o, 22.5^o$, and 45^0, and the nozzle pressure ratio, NPR=3.5, is shown in Fig.13. This illustrates an inessential dependence of noise on azimuthal direction. Small displacement of the SCR centerbody upstream, so that Screwdriver shape is started exactly from the throat cross section, did not reduce noise and produced only slight changes in the 1/3 octave band spectra. This is illustrated in Fig.14 where SCR corresponds to the standard centerbody location, as is shown in Fig.7a, and SCR-IN corresponds to the SCR design moved upstream. Comparisons are made for the two observation angles $\Theta = 30^o$ and 60^o, and two nozzle pressure ratios, NPR=1.6 and 3.5.

These experimental tests will be continued with the goal to obtain better acoustic results. In particular, we hope to improve acoustic characteristics by moving the centerbody into the nozzle and using penetrable walls for the SCR and/or the main nozzle. Preliminary results for such an approach are very promising.

III. Acoustic Tests of Bluebell Nozzles

Nine different Bluebell shaped nozzles were made at NASA LaRC and tested earlier, including the baseline round nozzle. The list of these nozzles, assigned numbers #1 thru #9, is represented in Table 1 along with their geometric parameters $n = n_p = n_c, \varepsilon, \delta_o$. Detailed information on Bluebell nozzle geometry is contained in several papers (see, for example, [3]). Note only that this geometry is defined by the three main parameters: $n = n_p = n_c, \varepsilon$, and δ_o. These give the frequency and amplitudes of the sinusoidal change of the nozzle lip-line edge denoted as "shevrons" (or petals) and the nozzle cross section shapes are denoted as "corrugations".

Table-1

No.	1	2	3	4	5	6	7	8	9
Ab.	**8C**	**8S**	**8S**	**8S**	**4C**	**4S**	**0R***	**8S**	**0R**
n	8	8	8	8	4	4	0	8	0
ε	0.23	0.23	0.38	0.15	0.45	0.45	0	0.23	0
δ_o	0.20	0.00	0.00	0.00	0.20	0.00	0	0.10	0

In Table 1, nozzle #7 is the round convergent baseline nozzle and nozzle #9 is the round convergent divergent baseline nozzle. Five of these nozzles, #1,2,5,6, and 9, were sent to TsAGI, Moscow. All of the nozzles have a throat radius r_*=0.637in (1.62cm) and the round nozzle has the exit radius r_c^o=0.694in (1.76cm). The Bluebell nozzles have exit radii defined by equation (1.2*b*). The length of the convergent part of all nozzles is x_*=2.05in (5.2cm) and the entire length of the baseline round nozzle is x_c^o=4.25in (10.8cm). All

of the Bluebell nozzle deisgns are based on the second formulation, with the use of additional sheets. Their lengths are varied from the baseline nozzle by an additional 1.0 to 1.1 inches depending on the geometrical parameters selected for the nozzle.

Abbreviations are introduced in the table for the tested nozzles: 8C and 8S are the 8-petal Blubell nozzles with corrugations ($\delta_o > 0$) and without corrugations ("skew", $\delta_o = 0$) respectively, and 4C and 4S are the same for the 4-petal Bluebell nozzles. Note, that during the tests at NASA SAJF, in the supersonic regime the nozzles were operated slightly underexpanded at the nozzle pressure ratio NPR=4.0 and jet total temperature $T_j = 350°F$. This corresponds to a fully expanded jet Mach number of 1.56 with corresponding exit velocity of 1740 ft./sec (531m/sec). All nozzles, except convergent nozzle 7, were designed for a fully expanded Mach number $M_e = 1.5$. This underexpanded condition was selected because it was expected that the nozzles with corrugations would reduce noise more effectively at this condition. In the subsonic regime the nozzles were operated at the nozzle pressure ratio NPR=1.27 and jet total temperature of $538°F$. This corresponds to an exhaust Mach number $M_e = 0.6$ with corresponding exit velocity 900 ft./sec (274m/sec). At either supersonic or subsonic nozzle operating conditions, the nozzles were sized to operate at the same ideal thrust.

The TsAGI acoustic tests were conducted with consecutive increases in total pressure, in the interval $1.6 \div 3.5$, that changed the jet issuing regime. In the interval of nozzle pressure ratios, $1.0 \leq NPR \leq 1.89$, a subsonic regime is always realized. Recall, that the reference round nozzle #9 is a convergent-divergent nozzle designed for a fully expanded exit Mach number, $M_e = 1.5$, with the rated nozzle pressure ratio, NPR=3.67. Therefore, in the overcritical nozzle pressure ratios interval, $1.89 \leq NPR \leq 3.67$, the gas flow is supersonic downstream of the nozzle throat. Static pressure increase then produces some oblique shock waves with a regular reflection from the nozzle-jet axis or with an irregular reflection forming a Mach disk at the axis. Shock waves are formed outside the nozzle creating a jet barrel-shaped structure. Stabilization of the shock waves inside a divergent nozzle portion is usually not observed. In an interval of $NPR \geq 3.67$, the jet is underexpanded and the barrel-shaped structure is present.

The main results of the TsAGI Bluebell nozzle acoustic tests are collected in Fig.6. Narrow band spectra of jets issuing from the five supersonic nozzles with the same mass flow rate are presented with the three nozzle pressure ratios: **NPR**= 1.6, 2.4, and 3.5, and three observation angles, $\Theta = 30°, 60°$, and $90°$. Acoustic data for the reference round nozzle designed for an exit Mach number, $M_e = 1.5$, are shown by black lines and denoted as **0R** (nozzle **#9** from the table). Data for the 8-petal Bluebell nozzle (BN) without corrugations, **8S** (**#2**) are denoted by blue lines ; data for the 8-petal BN with corrugations, **8C** (**#1**), by yellow lines; data for the 4-petal BN without corrugations, **4S** (**#6**), by green lines; and data for the 4-petal BN with corrugations, **4C** (**#5**), by red lines. These spectral density graphics are drawn using the aforementioned analyzer (model 2032/Brul'&K'err Co.) and PC-286 computer which provided a narrow band spectrum with a band size $\sim \Delta f$=32Hz. The considered frequency interval was from 0kHz to 25kHz, although the measurement system allows an interval from 0kHz to 100kHz.

In general, the TsAGI acoustic test results for cold nondesigned jets have been confirmed by previous NASA tests showing that Bluebell nozzles provide some acoustic benefits, especially in the direction of maximum noise production (for an observation angle, $\theta = 30°$). For the subsonic regime, NPR=1.6, these benefits are observed in all observation angles for all Bluebell nozzles, excluding nozzle #5 (4C) in an interval [0,5]kHz. The best design in this regime is nozzle #2 (8S). Recall that comparison in the subsonic regime is made with the reference round nozzle, #9, designed for the supersonic exit velocity with Mach number, $M_e = 1.5$. In accordance with quazi-one-dimensional inviscid theory, for such a nozzle with nozzle pressure ratio, NPR=1.6, the exit Mach number would be equal to $M_e = 0.8477$. Application of this theory for a Bluebell nozzle is generally not valid, especially near the corrugated exit. However, in these cases, the flow regime remains subsonic.

In the overcritical regime for nozzle pressure ratio, NPR=2.4, the reference round nozzle is overexpended. Strong shock wave formation in the exhaust jet leads to the presence of narrow discrete component (acoustic picks) in these spectra for all three observation angles. It is remarkable that these picks are not observed for all Bluebell nozzles. It is hoped that this is not the result of errors connected with the imperfect data processing apparatus. Similar acoustic picks were observed in other experiments with the round nozzles. We can conclude that this shock wave system was destroyed by using corrugated nozzle shapes. This effect occurred for both designs with and without corrugations. Unfortunately, a fully corrugated design without petals was not made and it can not be definitely determined which feature is particularly responsible for this effect, the presence of petals or corrugations. This will be studied further in the future. However, it may be asserted that the presence of only petals at the nozzle exit leads to the elimination of these picks in the narrow band spectra. The overall pressure level acoustic benefits of the Bluebell nozzles are essentially smaller in this regime than in the previous subsonic regime. The best designs are the 8 and 4-petal corrugated nozzles, #1 and #5.

In the near-designed regime of the issuing jet with

nozzle pressure ratio, NPR=3.5, acoustic benefits are observed only for the observation angle, $\theta = 30^o$. In this case, very weak shock waves are formed downstream of the nozzle exit and the narrow band spectra do not show any acoustic picks which were observed in the previous regime. Moreover, for the observation angle, $\theta = 90^o$, an increase in the noise level is observed. This result was surprising because the analogical NASA tests with closed conditions for slightly underexpanded supersonic hot jets have shown essential acoustic benefits from Bluebell nozzle application in the spectra interval, [0,20]kHz.

Thus, analysis of the Bluebell nozzle acoustic tests with cold jets at TsAGI (Moscow) have shown some additional effects which were not observed earlier during NASA LaRC acoustic tests with hot near-designed jets. Simultaneously, these tests bring to light some issues which require resolution. In particular, fabrication of an additional small scale Bluebell nozzle with corrugations and without petals, as well as the performance of identical tests with cold jets at NASA LaRC and TsAGI (Moscow) for proper comparison of results.

Numerical Simulation Results

Aeroperformance effects and gas dynamics flow characteristics were analyzed numerically. The nozzle thrust calculation were based on a full Navier-Stokes equations solver (NSE), and both full and marching Euler codes: CFL3D [7], CRAFT [8], and Krayko-Godunov [9]. Grid preparation and optimization was conducted using GRIDGEN and our own codes. The main results were obtained using 2D and 3D versions of the CFL3D code which allows the simulation of both inviscid and viscous flows. This code is described in detail in the CFL3D User's Manual (Version 5.0) [10]. In accordance with this manual introduction ([10], page 1): " ...CFL3D (Version 5.0) is a Reynolds-Averaged thin-layer Navier-Stokes flow solver for structure grids... CFL3D solves the time- dependent conservation law form of the Reynolds-averaged Navier-Stokes equations. The spatial discretization involves a semi-discrete finite-volume approach.

Upwind-biasing is used for the convective and pressure terms, while central differencing is used for the shear stress and heat transfer terms. Time advancement is implicit with the ability to solve steady or unsteady flows. Multigrid and mesh sequencing are available for convergence acceleration. Numerous turbulence models are provided, including 0-equation, 1-equation, and 2-equation models. Multi-block topologies are possible with the the use 1-1 blocking, patching, overlapping, and embedding. CFL3D does not contain any grid generation software. Grids must be supplied extraneously."

In Figures 16-23 some numerical results are presented. In Fig. 16a,b Cartesian (x, y, z) and cylindrical (z, r, θ) coordinate systems and a typical 3D grid are shown with indicies (i, j, k) running from (1,1,1) to $(idim, jdim, kdim)$ in a normalized rectangular 3D region. This grid was used for numerical simulation of the supersonic nozzle with the 4-petal Screwdriver shaped centerbody (plug). The region of direct calculation is limited by 6 boundaries with the following boundary conditions: **1)** In the θ direction by the two planes of symmetry $\theta = 0^o$ (z=0) and $\theta = 45^o$ with the boundary conditions for symmetry planes (or conditions for an inviscid flow on a solid surface). **2)** In the x direction by the two cross section planes, x=0 (inlet), and $x = x^e$ (exit). At the inlet so called "inflow/outflow" ([8]) inviscid boundary conditions are used which define all of the non-dimensional flow parameters if pressure and temperature ratios are given. Here, 1D Riemann invariants are applied in the direction normal to the boundary. At the exit, extrapolation boundary conditions are used which are cell-center type boundary conditions. **3)** In the radial r direction, either inviscid or viscous solid wall conditions are imposed.

Initially, the numerical calculations focused on the simulation of the inviscid and viscous flow issuing from jets having axisymmetric and Screwdriver centerbodies. However, these geometries provide several features which make performing such calculations difficult. Therefore, computations were performed which focused on the nozzle portion of the flow to gain some experience and provide some understanding of the issues involved in the full jet simulations. While many of the results are preliminary, it is useful to study some results and conclusions. Figure 17 illustrates some results for viscous flows (using Menter's $k-\omega$ SST turbulence model [11]). within nozzles having axisymmetric and Screwdriver centerbodies (nozzle pressure ratio NPR = p_o/p_∞ = 2.296 and nozzle temperature ratio NTR = T_o/T_∞ = 2.817). Figures 17b and 17c show the mach contours for the axisymmetric centerbody and the $\theta = 45^o$ plane for the Screwdriver centerbody. The general profile of the two flows is similar, as also seen in figures 17d and 17e, which provide some indication of the flow near the surface of the centerbody.

One of the issues of interest was the introduction of vorticity to the nozzle flow by the Screwdriver centerbody, as opposed to a simple axisymmetric centerbody. Figures 18a, b, and c provide some illustration of the general viscous flow within the nozzle. Figures 18d and 18e show the mach contours at the nozzle exit for an inviscid and viscous case. Superimposed on these contours are flow streamlines which show a considerable change in the flow field for the inviscid and viscous cases. While some of this vorticity may be generated by the numerical scheme itself, it would be hoped that some vorticity is actually generated by the presence of the Screwdriver centerbody, leading to enhanced mixing.

In figure 19, the results from studying the influence of the axisymmetric centerbody location on the inviscid flow field within the nozzle are presented. In looking at the mach contours, it may be seen that movement of the centerbody toward the throat produces shock waves which are reflected downstream. In this case, however, this strong shock structure does not greatly effect the thrust production.

With experience from the nozzle calculations in hand, numerical simulations of some full jet flows were performed. Figure 20 shows results for an inviscid jet, with an axisymmetric centerbody, employing two different computational grids. In this figure, grid 1 corresponds to a coarse grid with dimensions 162 × 66 in the i and j directions, respectively. Grid 2 is a much finer grid with dimension 306 × 154. The residual history shows that the coarse grid calculations converges much better than the fine grid calculation. The comparison of the mach contours seem to indicate that this behavior may be the result of problems at the outflow boundary. In this region, a large flow gradient is present which may lend to some instability.

Simulation results for a jet with a Screwdriver centerbody are included in figure 21. It appears that there is more mixing in this case. However, as in figure 20, it may be seen that the solution is not fully converged. This may again be caused in part by difficulties at the jet outflow boundary. This case may however provide some insight into the form of the flow field. Figure 22 shows mach contours and streamlines for this inviscid flow on the surface of the Screwdriver centerbody. It can be seen that this flow incorporates flow features which would not be present with an axisymmetric centerbody.

One final area of interest is the effect of the centerbody geometry on thrust. Figure 23 presents the drag produced by the subsonic portion of the nozzle minus the thrust produced by the centerbody. Studying this "effective" drag provides an indication of the thrust production with various centerbody geometries. The preliminary conclusions of this numerical analysis indicate that the nozzle with the SCR plug provides less thrust than the nozzle with the impenetrable CON plug by a factor of ~1-2%. Detailed graphic visualization of the gas flow in the nozzle and exhaust jet have revealed some important acoustic effects in the experiments conducted. With the experience gained from these preliminary calculations, it is hoped that further numerical simulations will provide insight into the study of these jet flows.

Conclusions

Several different corrugated designs, including Screwdriver shaped centerbodies and Bluebell nozzles were tested experimentally and numerically. Acoustic tests conducted at TsAGI, Moscow and numerical simulations at NASA LaRC have provided preliminary results which indicate that the tested Screwdriver shaped centerbody did not produce the expected acoustic and aeroperformance benefits. Acoustic tests performed on the Bluebell nozzles essentially confirmed, in general, previous NASA LaRC experiments which show acoustic benefits from these designs (including subsonic regimes).

Acknowledgements

This work is a portion of research being carried out under NASA Grants NAG-1-1835, 1936 and CRDF Grant RE2-136. The authors would like to express their appreciation to the NASA LaRC Jet Noise Team for their support and Dr. John M. Seiner for his supervision on all of these projects. Thanks also to Dr. Dennis M. Bushnell for his interest in our research.

References

1. Seiner, J.M., and Gilinsky, M.M., 1993, A Bluebell Nozzle for Improving the Mixing of Exhaust Jets with Ambient Air, Invention Disclosure, NASA Case No. LARC-15215-1.

2. Seiner, J.M., and Gilinsky, M.M., 1995, "Nozzle Thrust Optimization while Reducing Jet Noise", CEAS/AIAA Paper 95-149, 1st Joint CEAS/AIAA Aeroacoustics Conf., June 12-15,1995, Munich, Germany.

3. Seiner, J.M., and Gilinsky, M.M., 1997, Nozzle Thrust Optimization while Reducing Jet Noise, AIAA Journal, Vol.35, No. 3, pp. 420-427.

4. Gilinsky, M.M., and Seiner, J.M., 1996, Corrugated Nozzles for Acoustic and Thrust Benefits of Aircraft Engines, CEAS/ AIAA Paper 96-1670, 2nd CEAS/AIAA Aeroac. Conf., May 6-8, State College, PA.

5. Kouznetsov, V.M., Munin, A.G, et al., 1981, Aerodynamic noise sources, Moscow, Publ. "Mashinostroenie", 248p.

6. Bushgens, G.S., and Bedrjitsky, E.L., 1993, TsAGI-Aviation Science Center, Moscow, "Nauka", 272p.

7.Rumsey, C.L., et al., 1995, Efficiency and Accuracy of Time-Accurate Turbulent Navier-Stokes Computations, AIAA Paper 95-1835, 13th AIAA Applied Aerodynamics Conference, June 19-22, 1995/San Diego, CA.

8. Molvik, G.A. and Merkle, C.L. 1989, A Set of Strongly Coupled, Upwind Algorithms for Computing Flows in Chemical Nonequilibrium, AIAA Paper 89-0199, 27th Aerospace Sciences Meeting, Jan. 9-12.

9. Godunov, S.K. et al., 1976, Numerical Solution of Multidimensional Problems of Gas Dynamics, Moscow: Nauka, 1976, 400p.

10. Krist, S.L., Biedron, R.T., and Rumsey, C.L., 1996, CFL3D User's Manual (Version 5.0), NASA Langley Research Center, 311p.

11. Menter, F. "Improved Two-Equation $k-\omega$ Turbulence Models for Aerodynamic Flows," NASA TM 103975, 1992.

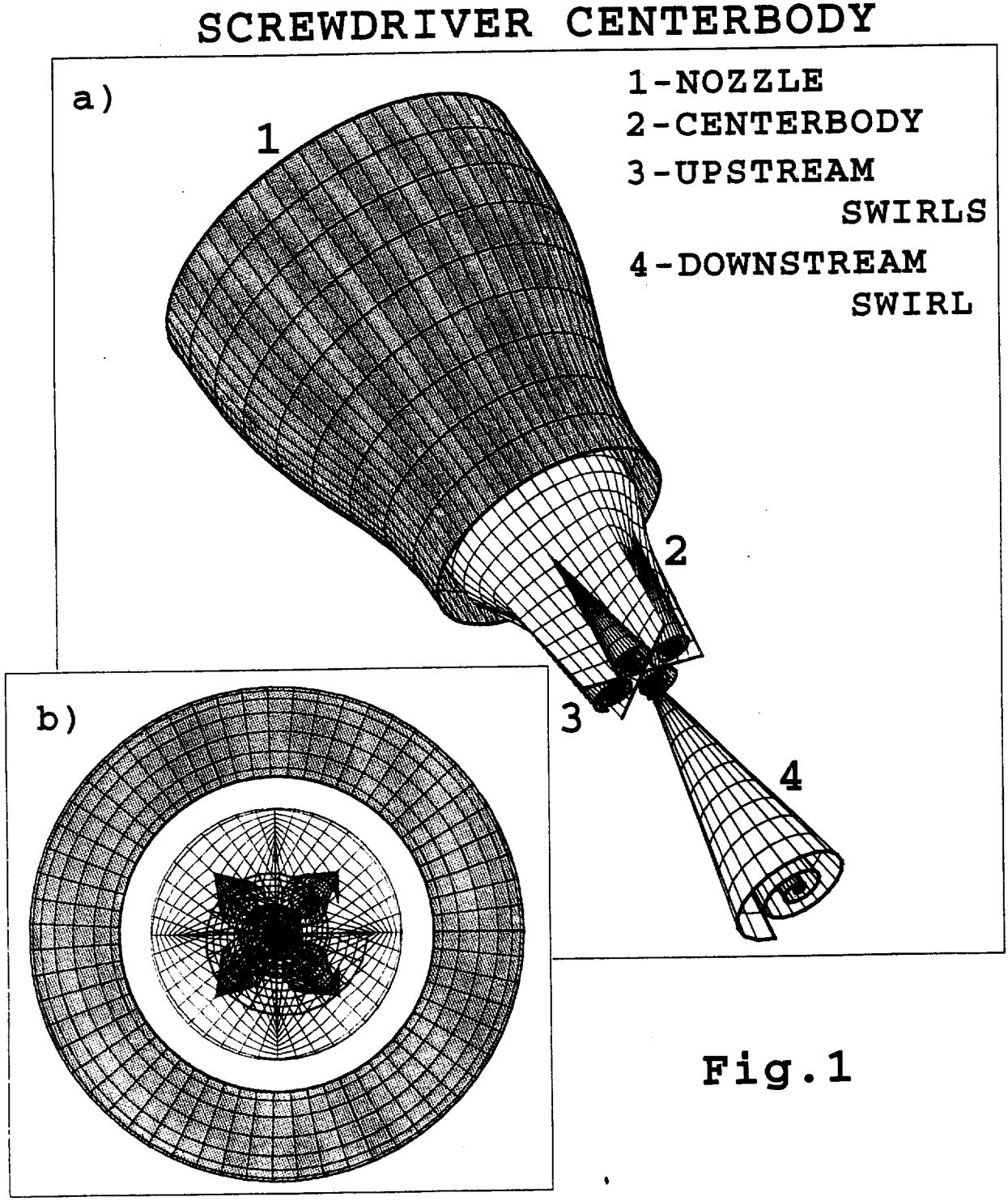

Fig.1

Fig.1 A Screwdriver centerbody (plug). a) -3D lateral view: 1 - nozzle, 2 -centerbody, 3 -upstream swirls at the line of symmetry, 4 -downstream swirl behind a centerbody along the axis of symmetry; b) - up-view from downstream.

DIFFERENT MODIFICATIONS OF SCREWDRIVER CENTERBODIES

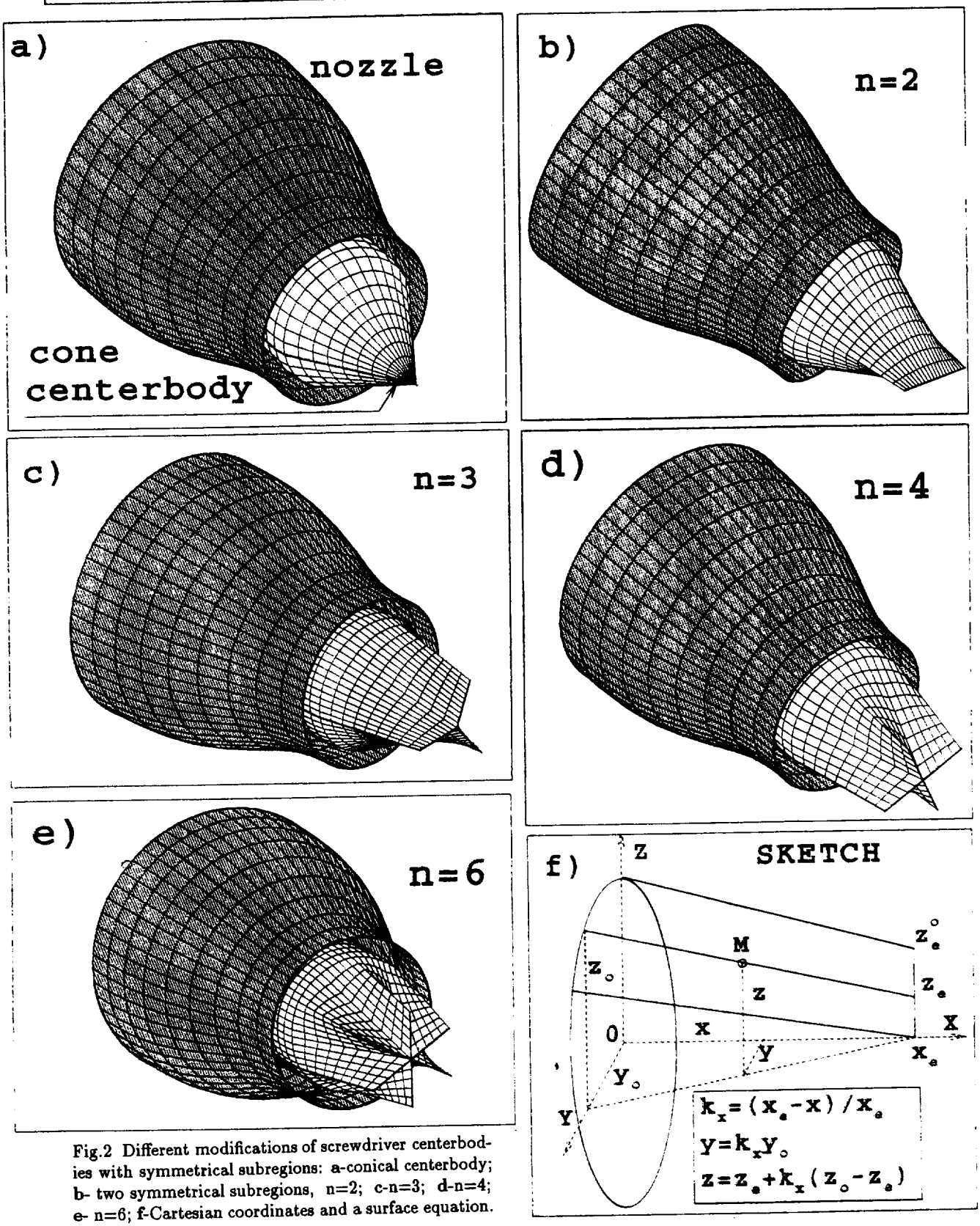

Fig.2 Different modifications of screwdriver centerbodies with symmetrical subregions: a-conical centerbody; b- two symmetrical subregions, n=2; c-n=3; d-n=4; e- n=6; f-Cartesian coordinates and a surface equation.

Fig.2

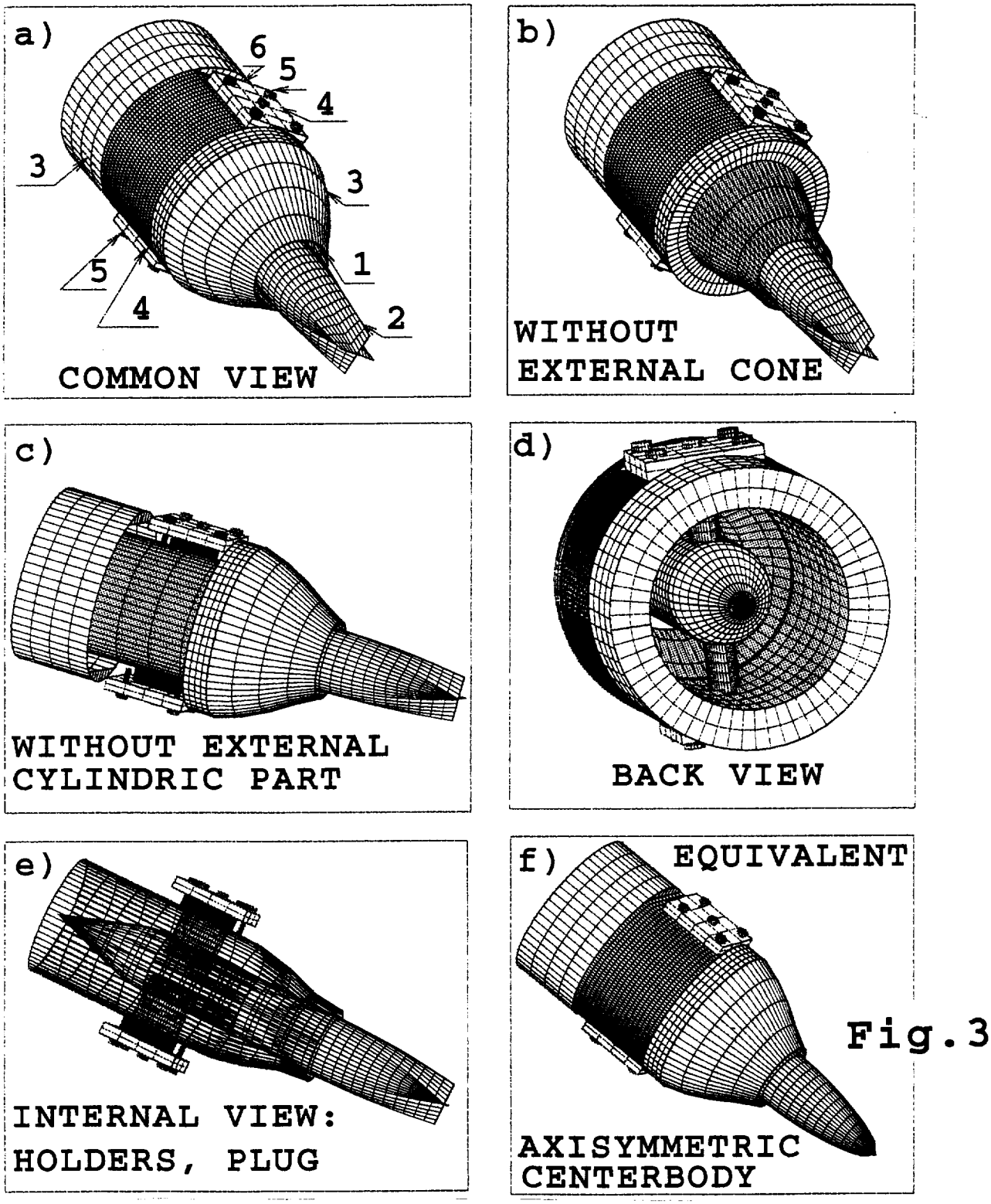

Fig.3

Fig.3 A Sonic nozzle with the Screwdriver Centerbody as a unit. The model was drafted for experimental tests at the TsAGI, Moscow.

a) common view: 1-sonic nozzle throat, 2-Screwdriver centerbody, 3-external nozzle surface, 4- plate to keep the holders, 5-bolts to keep the plate and to compress the holders, 6-plane ground for the plate;

b) view without the external cone; c) lateral view without the external cylindric part; d) back view; e) internal view without some shades; f) axisymmetric centerbody with the equal cross section areas as well as the Screwdriver centerbody.

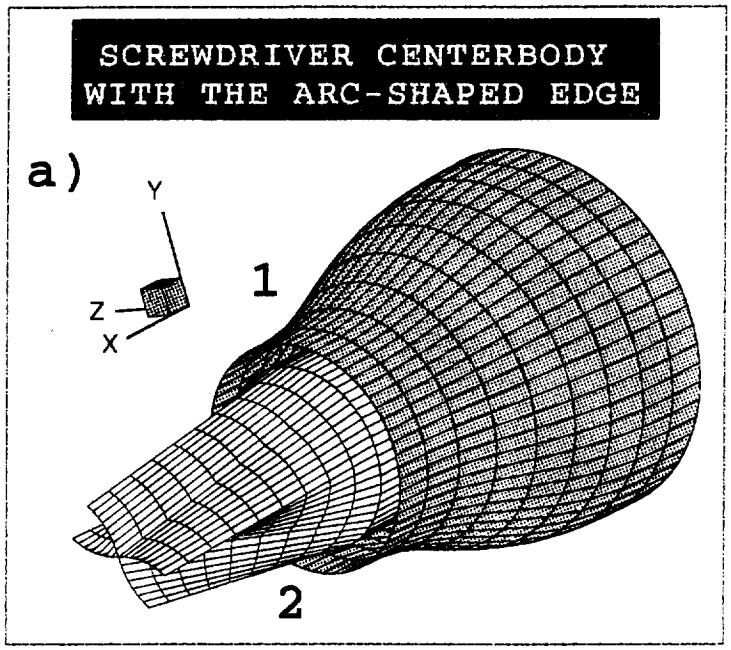

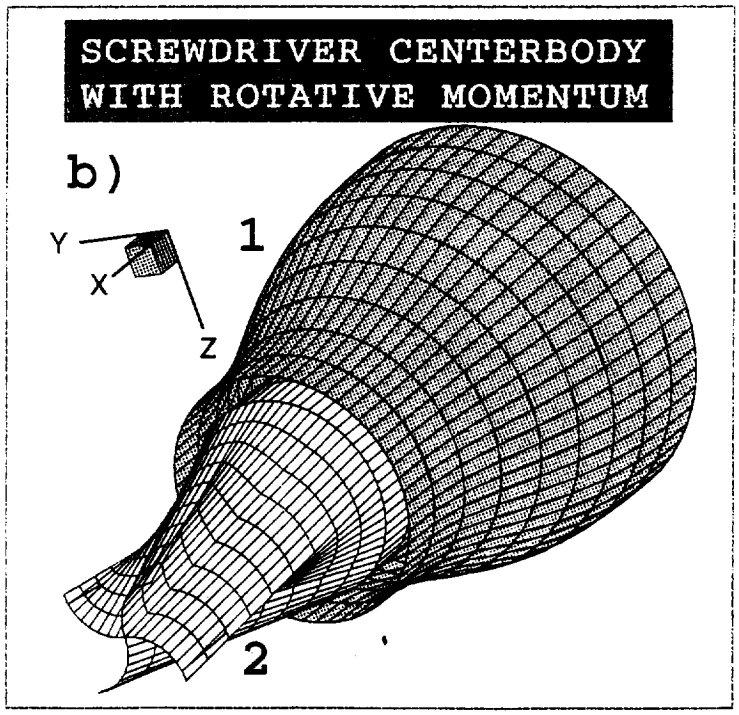

Fig.4

Fig.4 4-petal Screwdriver centerbody (plug). **1** - nozzle, **2** -centerbody. **a)** -Srewdriver centerbody with the arc-shaped edge, symmetrical location of petals without a lift and momentum. **b)** -Screwdriver centerbody (plug) with a rotative momentum.

Chisel centerbody (afterbody) geometry.

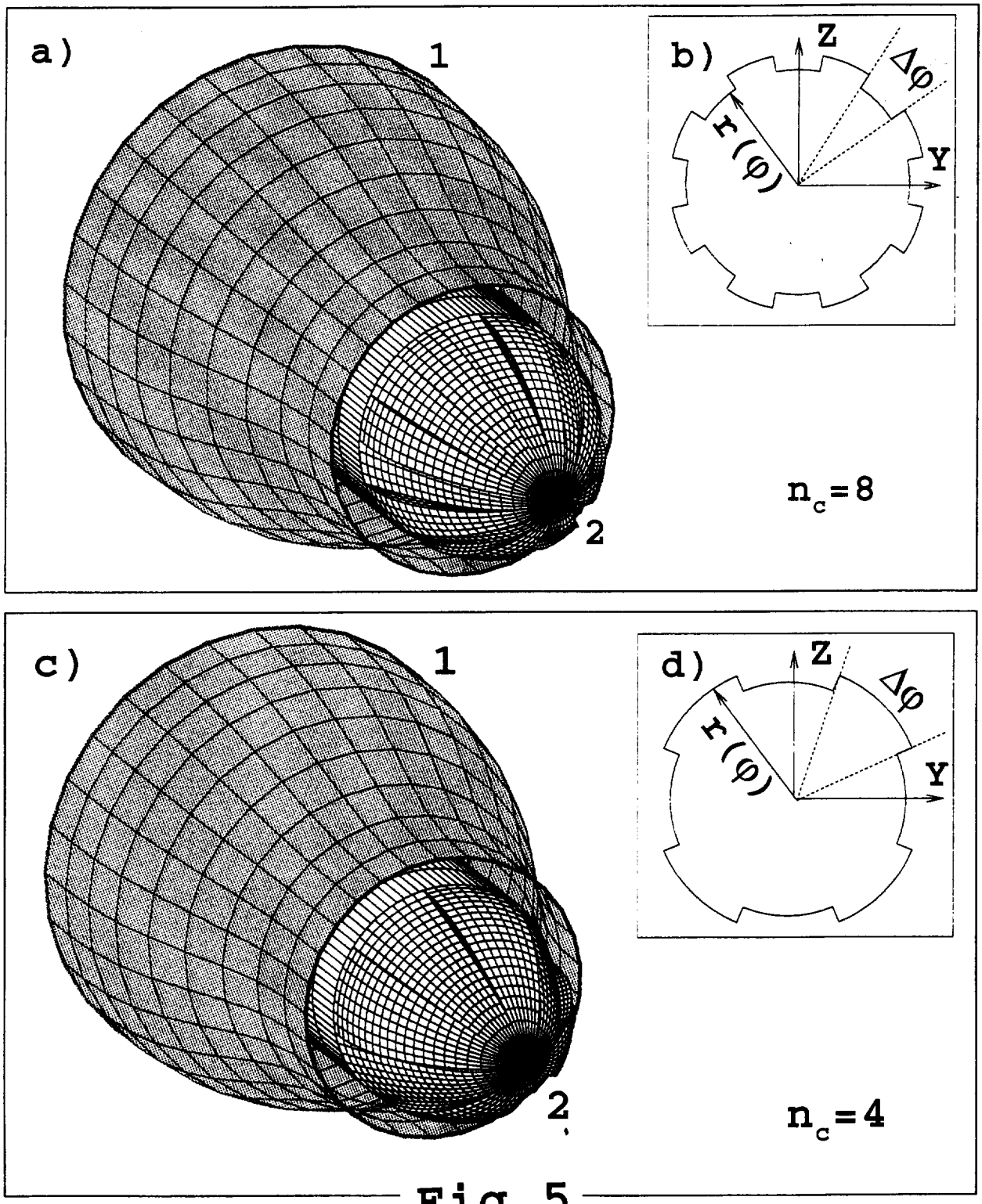

Fig.5

Fig.5 A Chisel centerbody (plug) geometry. 1) $n_c = 8$: a)-3D view, 1- nozzle, 2- centerbody. b)- centerbody cross section. 2) $n_c = 4$: c)-3D view, 1- nozzle, 2- centerbody. d)- centerbody cross section.

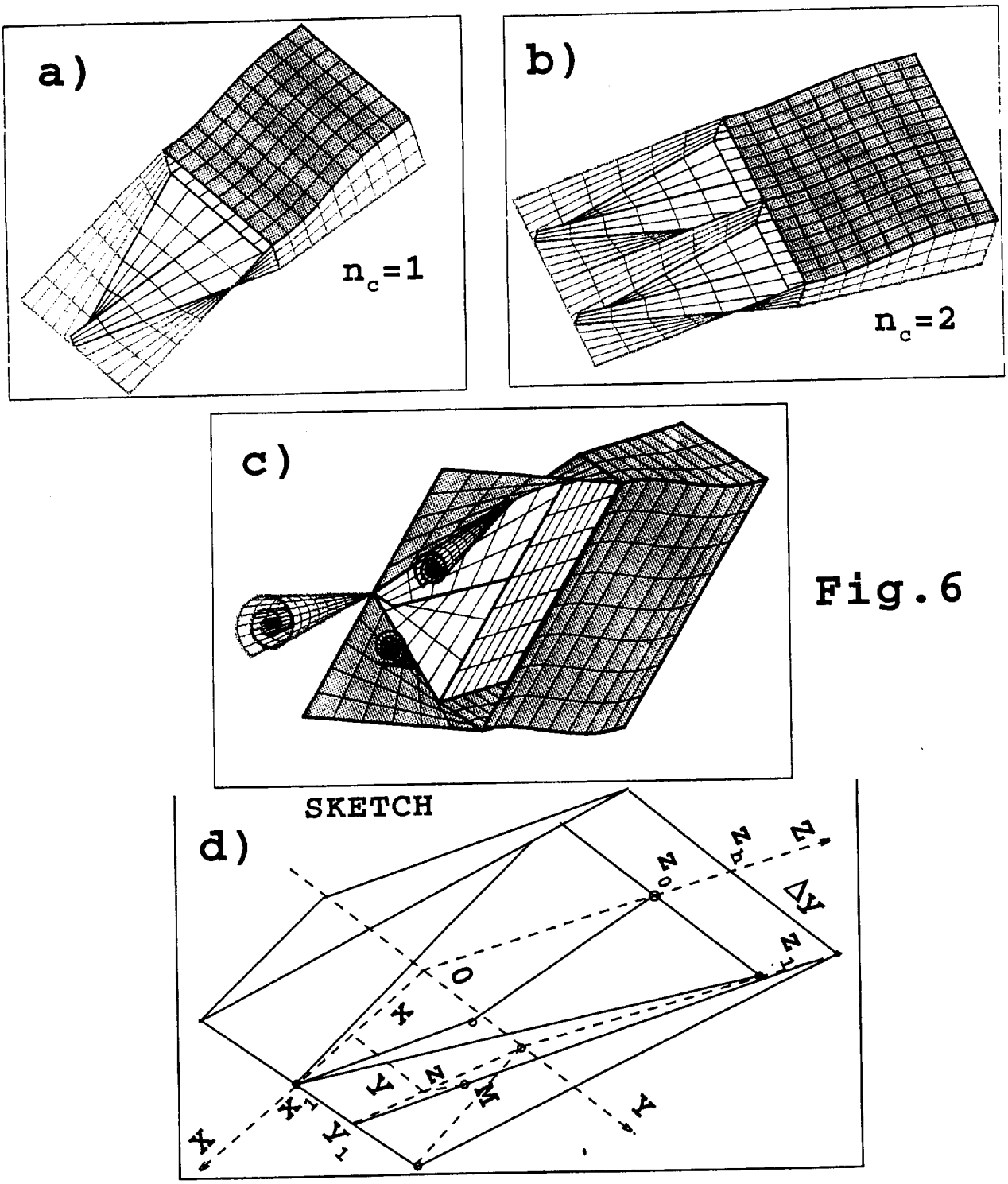

Fig.6

Fig.6 A 2D analogue of an axisymmetric Screwdriver centerbody (or a plug).

a) -a single 2D element of the nozzle (n_c=1). A surface of the supersonic part is linear: the yellow element contains straight lines (red), which join points of the throat horizontal side with the vertical interval at the nozzle (or the plug) edge; the two white elements contain straight lines (blue), which join points of the throat vertical sides with the two horizontal half-intervals at the nozzle (or the plug) edge. b) - a two-contour element (n_c=2). c)-Schematic swirls into a 2D Screwdriver nozzle cell flow; d)- surface geometry.

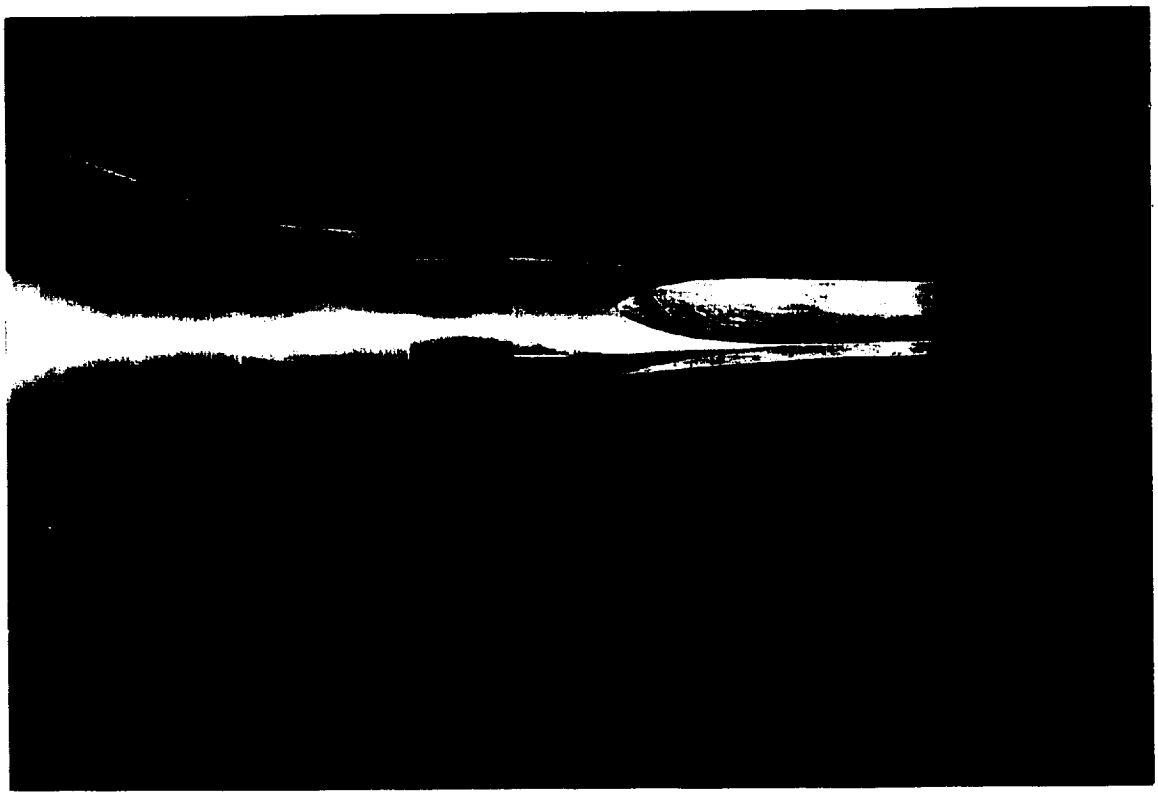

Fig.7

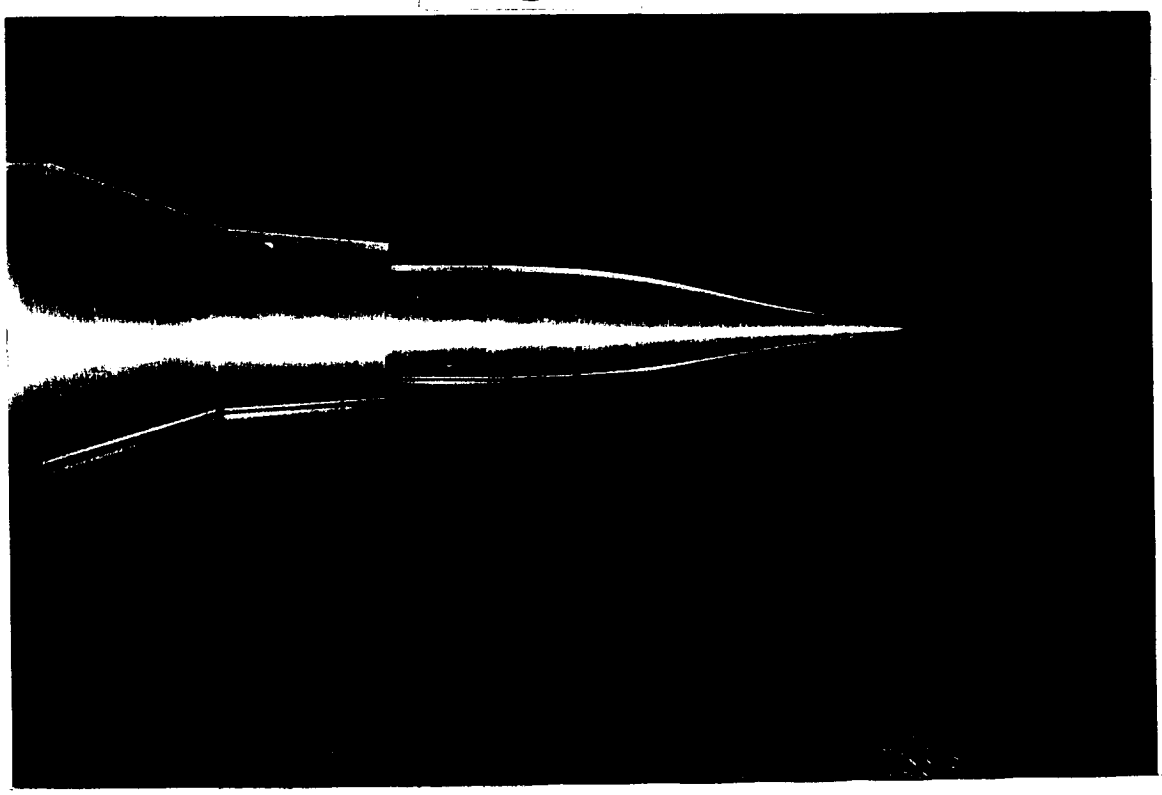

Fig.7 Axisymmetric convergent-divergent nozzle with the Screwdriver-shaped (a) and axisymmetric (b) centerbodies. Both centerbodies have the same areas at the cross section located on the same distance, $x = x_i$=const, from the throat, $x = 0$. These designs were tested in the anechoic chamber at the TsAGI, Moscow.

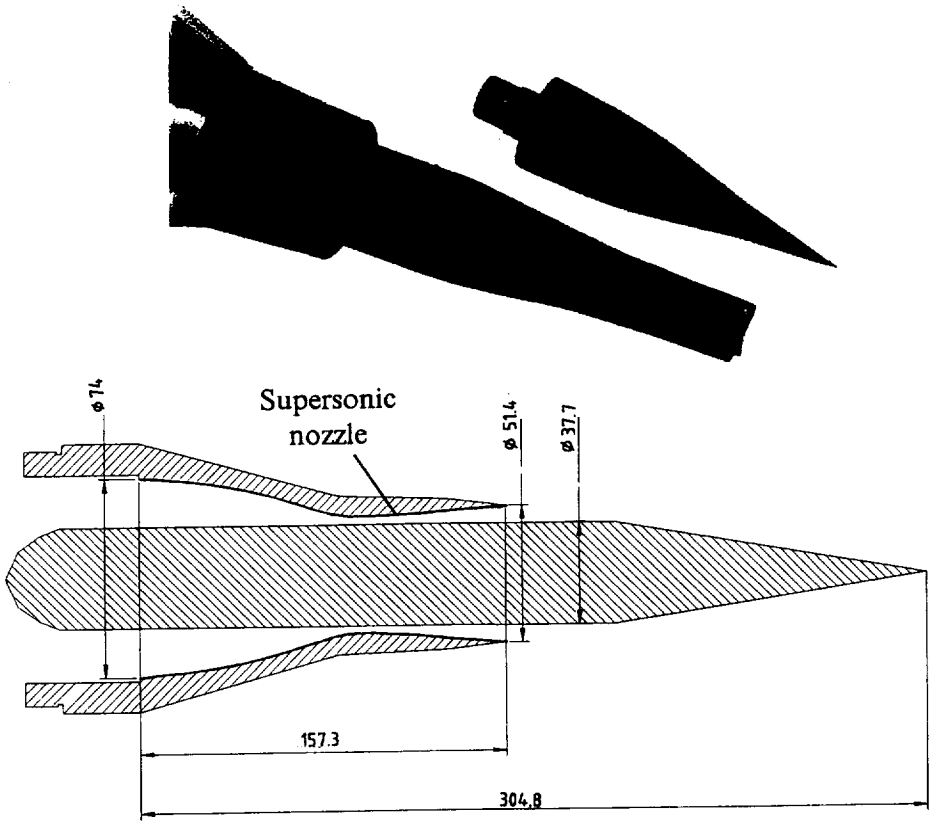

Fig.8 The picture of the nozzles with the Screwdriver-shaped (SCR) and axisymmetric (CON) centerbodies (a). The main sizes (mm.) of the nozzle CON (b).

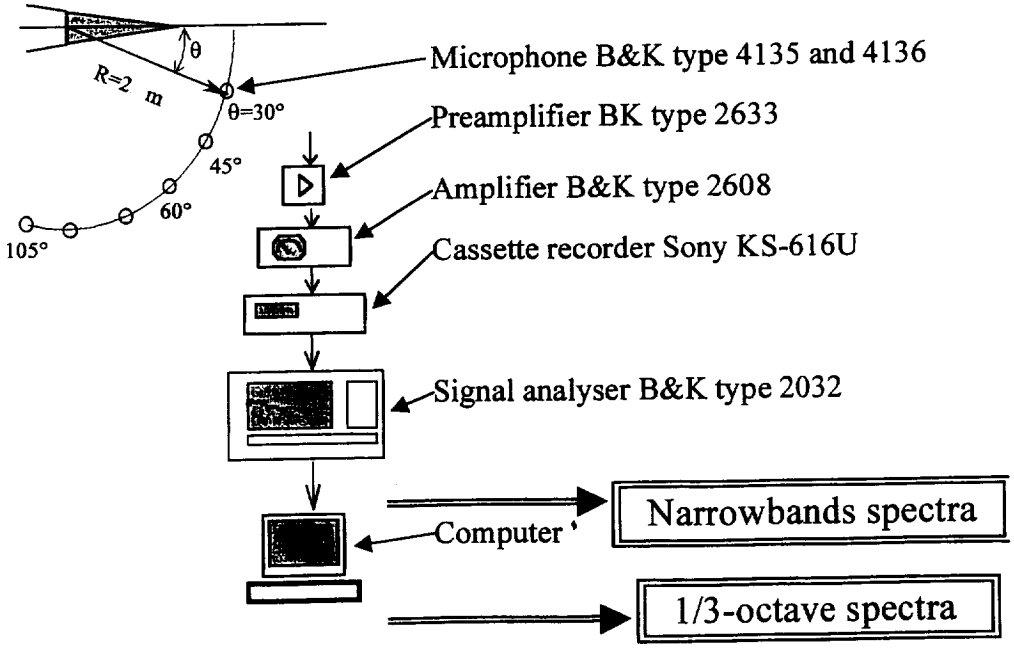

Fig.9 The scheme measurement in the anechoic chamber AK-2 at the TsAGI, Moscow, and the scheme of automatic data processing.

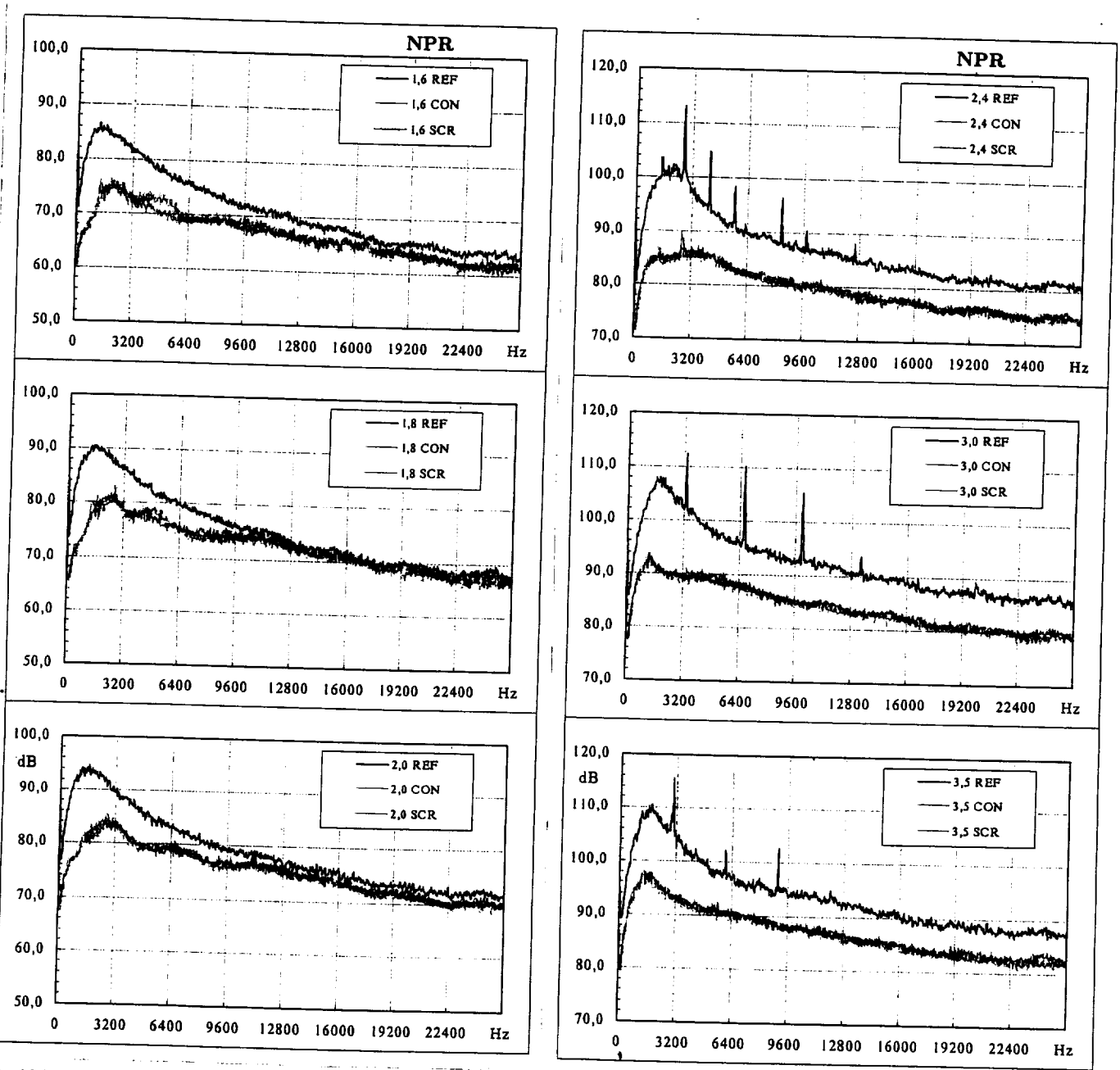

Fig.10 Narrowband spectra of jets issuing from the three supersonic nozzles with the same mass flow rate and with the nozzle pressure ratios, NPR= 1.6, 1.8, 2.0, 2.4, 3.0 and 3.5. Experimental results for the round nozzle without centerbody (REF) are shown by black lines, for the nozzle with the axisymmetric centerbody (CON) are shown by red lines, for the nozzle with the Screwdriver-shaped centerbody (SCR) are shown by blue lines. Observation angle, θ=30°.

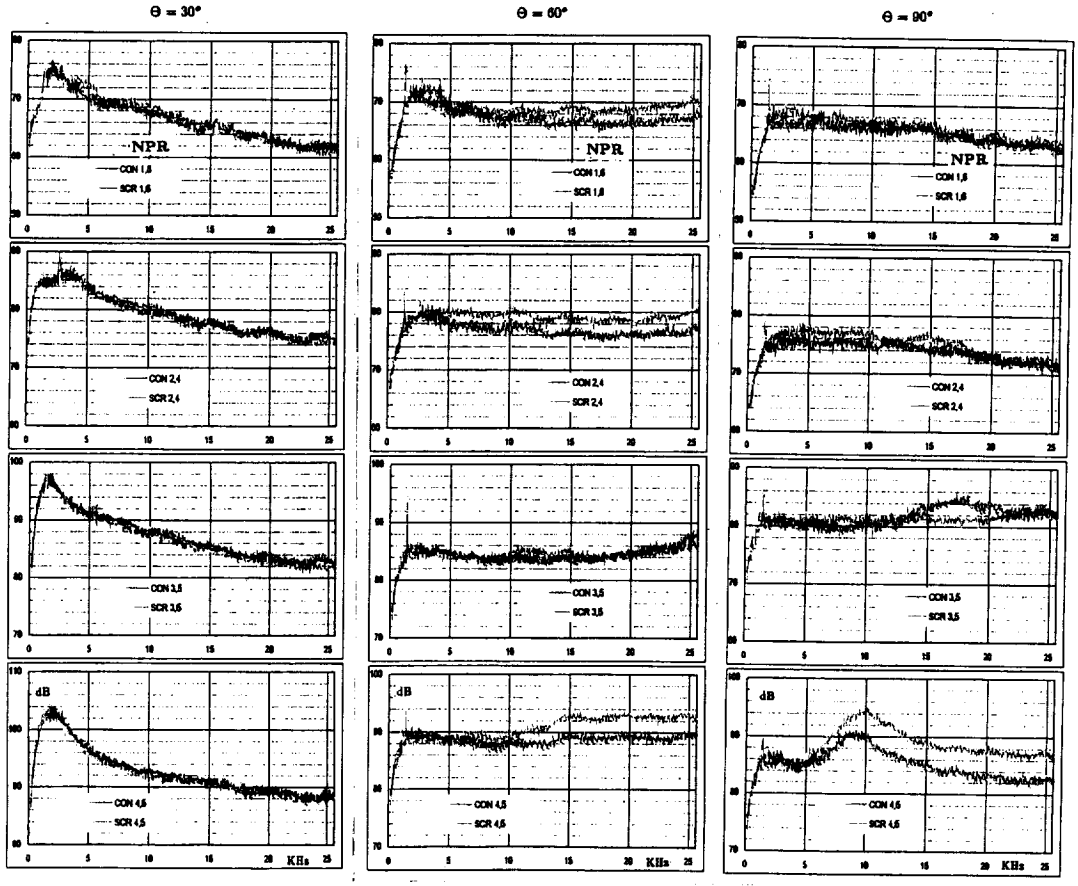

Fig.11 Narrowband spectra of jets issuing from the two supersonic nozzles with the same mass flow rate, with the four nozzle pressure ratios: **NPR**= 1.6, 2.4, 3.5 and 4.5, and three observation angles, $\Theta = 30^o, 60^o$, and 90^o. Experimental results for the round nozzle with the axisymmetric centerbody (CON) are shown by blue lines, for the nozzle with the Screwdriver-shaped centerbody (SCR) are shown by yellow lines.

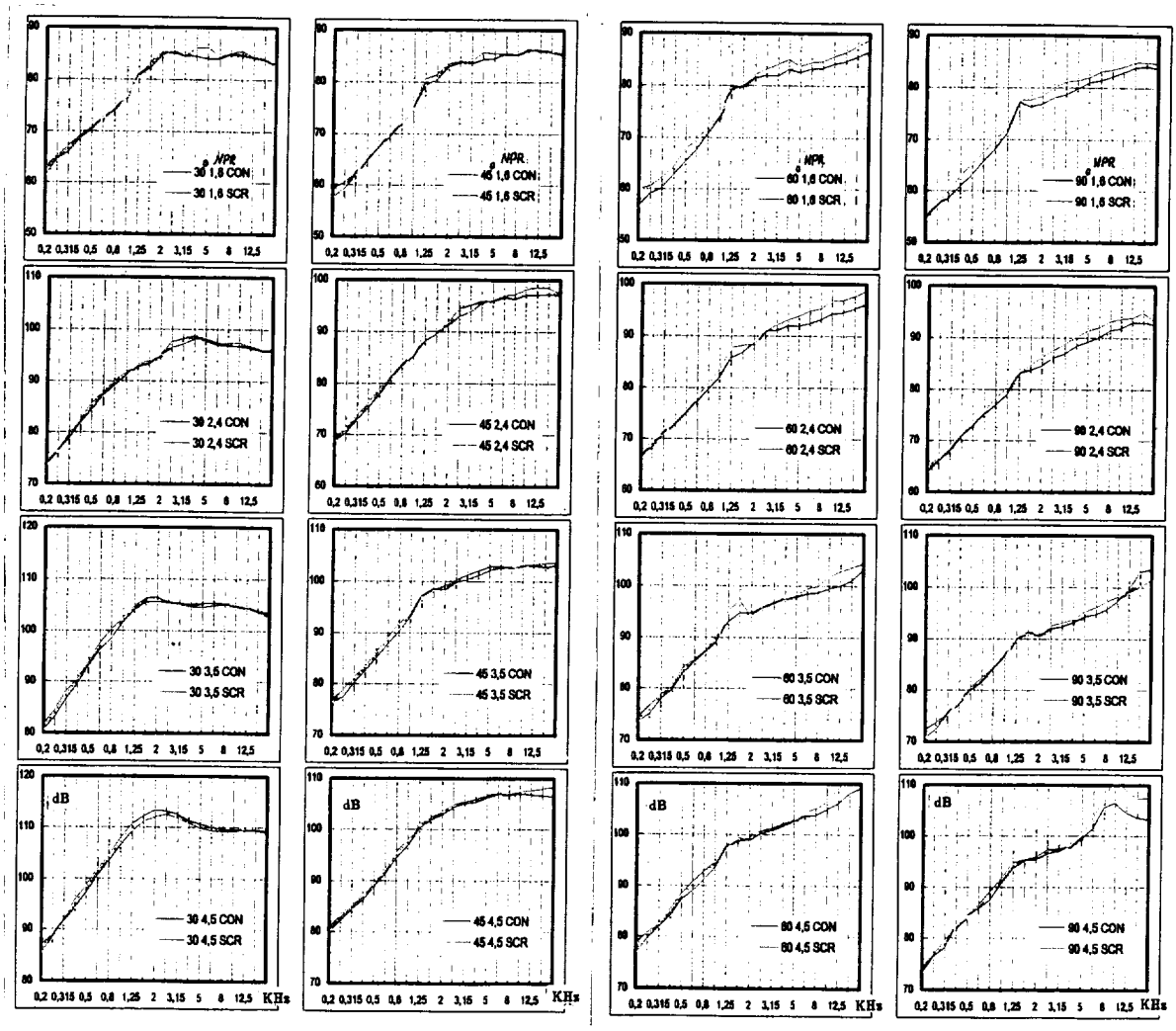

Fig.12 1/3-octave band spectra of jets issuing from the two supersonic nozzles with the same mass flow rate, with the four nozzle pressure ratios: **NPR**= 1.6, 2.4, 3.5 and 4.5, and four observation angles, $\Theta = 30^o, 45^o, 60^o$, and 90^o. Experimental results for the round nozzle with the axisymmetric centerbody (CON) are shown by blue lines, and for the nozzle with the Screwdriver-shaped centerbody (SCR) are shown by yellow lines.

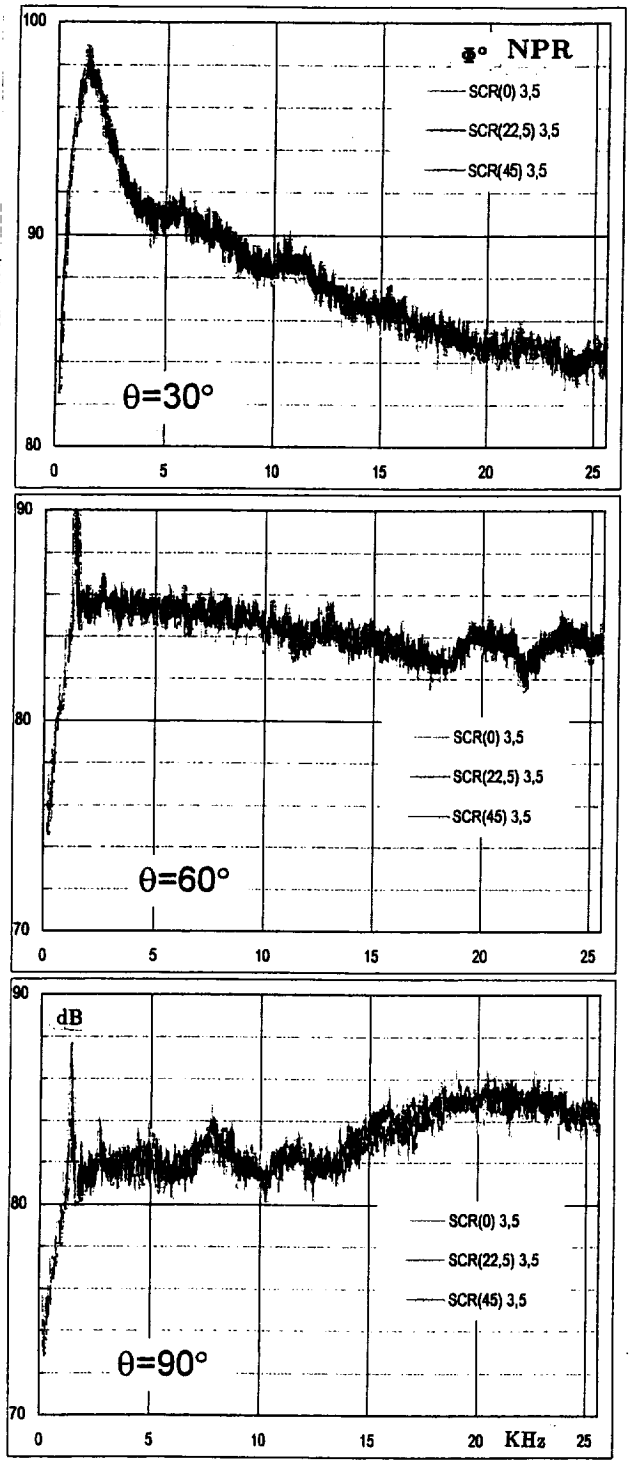

Fig.13 Influence of the azimuthal angle Φ on narrow-band spectra at the three observation angles, Θ = 30°, 60° and 90°, and nozzle pressure ratio, NPR=3.5.

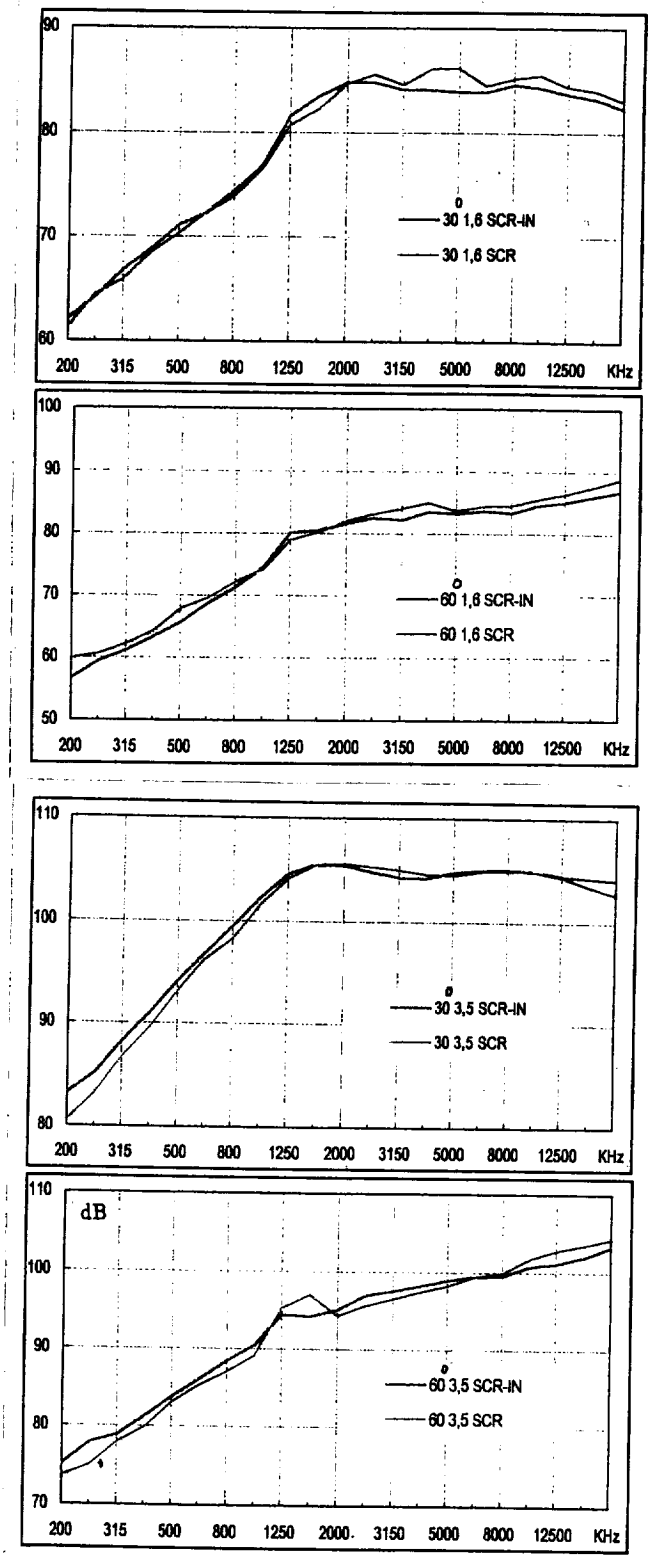

Fig.14 Influence of location of the Screwdriver-shaped centerbody on 1/3-octave band spectra for the two observation angles, Θ = 30° and 60°, and two nozzle pressure ratios, NPR=1.6 and 3.5. SCR-corresponds to standard location as is shown in Figure 7a, and SCR-IN-corresponds to the Screwdriver-shaped centerbody moved upstream so that Screwdriver shape is started

BLUEBELL NOZZLES ACOUSTIC TESTS (TsAGI, MOSCOW, CHAMBER AK-2)

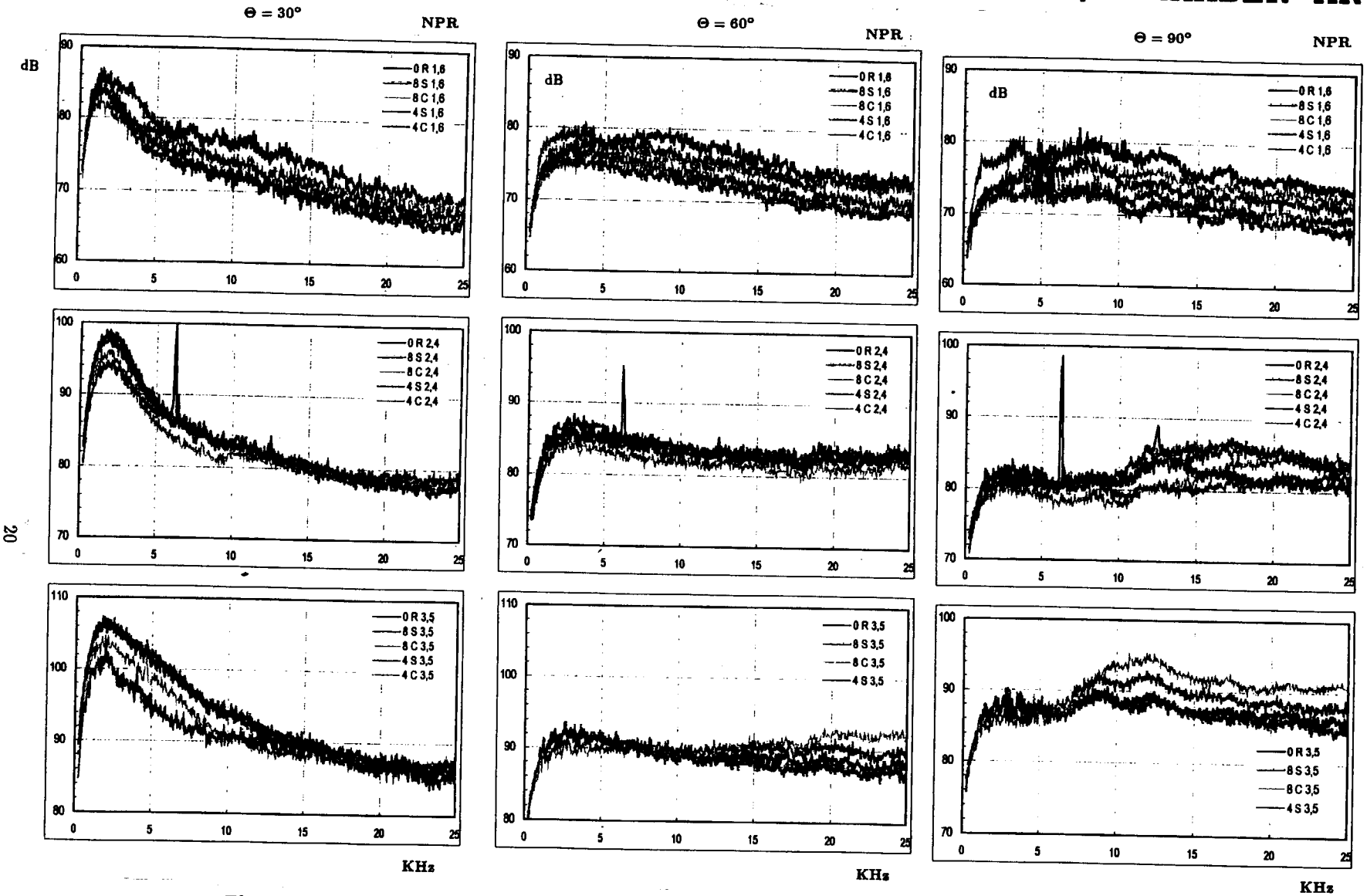

Fig.15 Narrowband spectra of jets issuing from the five supersonic nozzles with the same mass flow rate, with the three nozzle pressure ratios: **NPR**= 1.6, 2.4, and 3.5, and three observation angles, $\Theta = 30°, 60°$, and $90°$. Acoustic data for the reference round nozzle designed for an exit Mach number, $M_e = 1.5$, are shown by black lines and denoted as **0R** (nozzle #9) from the table); data for 8-petal Bluebell nozzle (BN) without corrugations, **8S** (#2), are by blue lines ; data for 8-petal BN with corrugations, **8C** (#1), are by yellow lines; data for 4-petal BN without corrugations, **4S** (#6), are by green lines; data for 4-petal BN with corrugations, **4C** (#5), are by red lines.

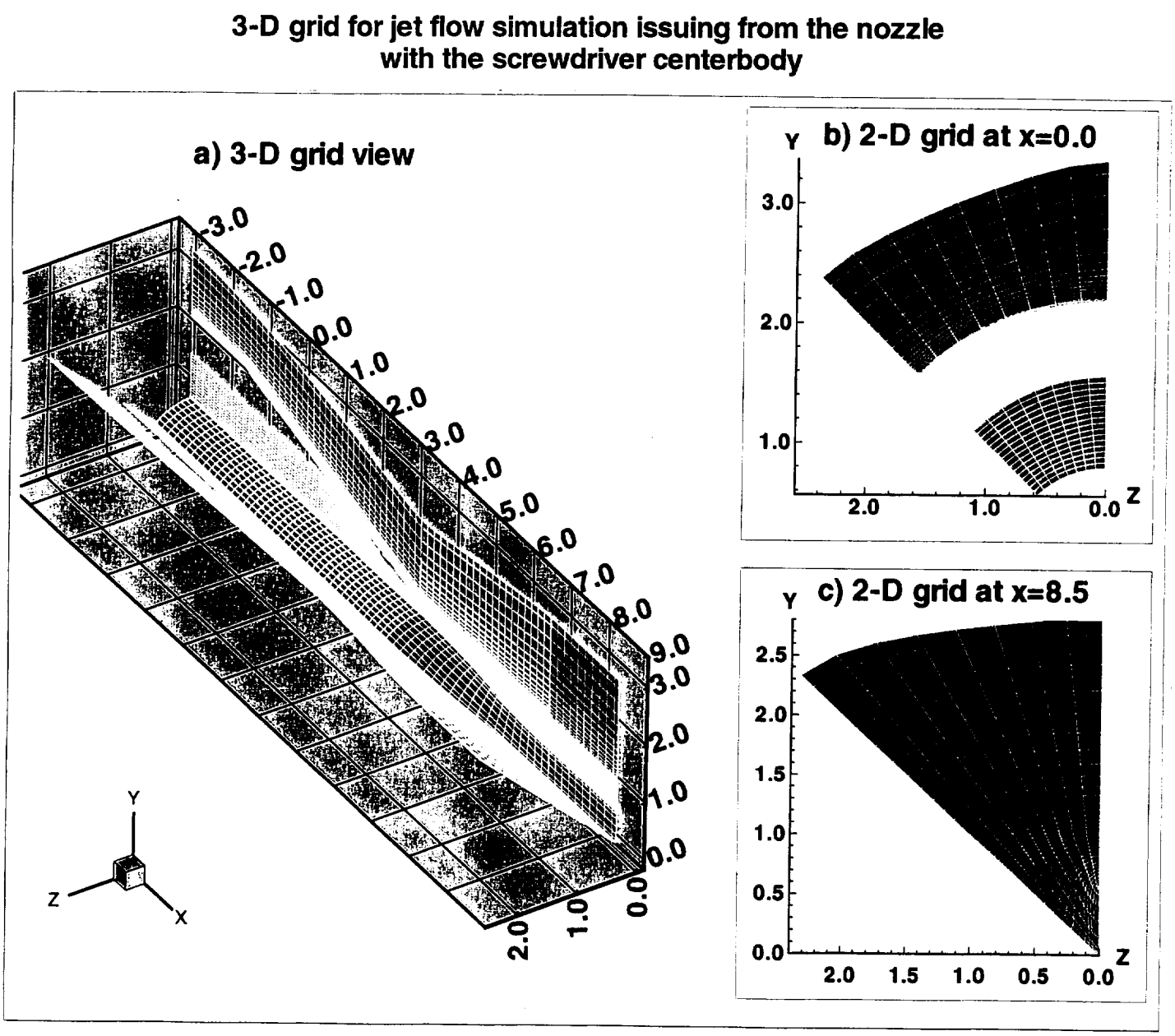

Fig. 16 3-D grid for jet flow simulation issuing from the nozzle with the screwdriver centerbody. **a)** 3-D grid view: in the XOY-plane, a plane of symmetry, $\theta = 45^o$, and on the centerbody's surface. **b)** 2-D grid at the inlet, x=0.0, where inlet flow conditions are specified. **c)** 2-D grid downstream of the end of the centerbody, x =8.5.

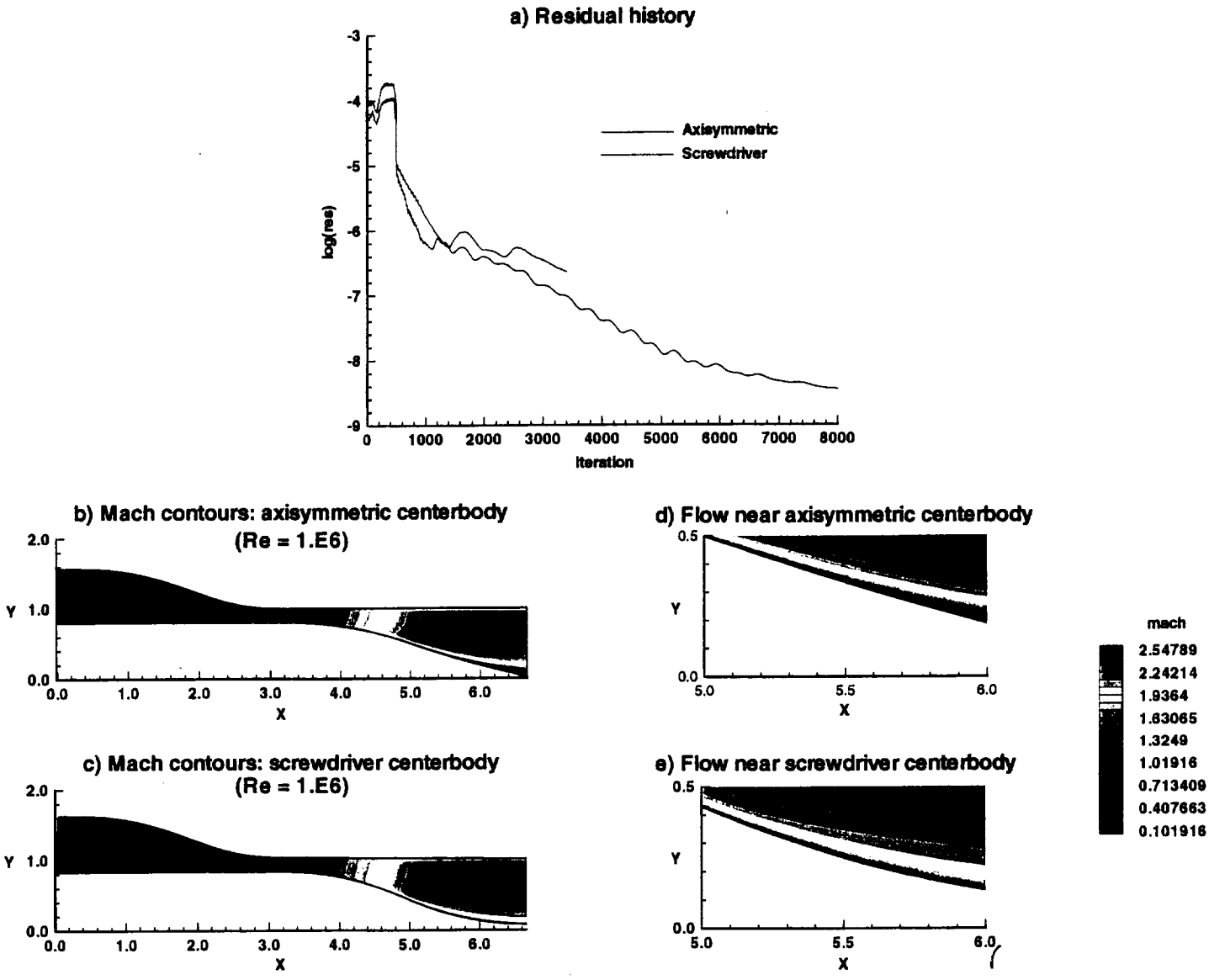

Fig. 17 Residual history and Mach contours for nozzles with axisymmetric and screwdriver centerbodies (nozzle pressure ratio NPR = p_o/p_∞ = 2.296, nozzle temperature ratio NTR = T_o/T_∞ = 2.817). **a)** Residual history for the two cases. **b)** and **c)** Results of Navier-Stokes simulations with the two types of centerbody. **d)** and **e)** Illustration of the flow profile near the centerbody surfaces.

Mach Contours for viscous and inviscid nozzle flow simulations

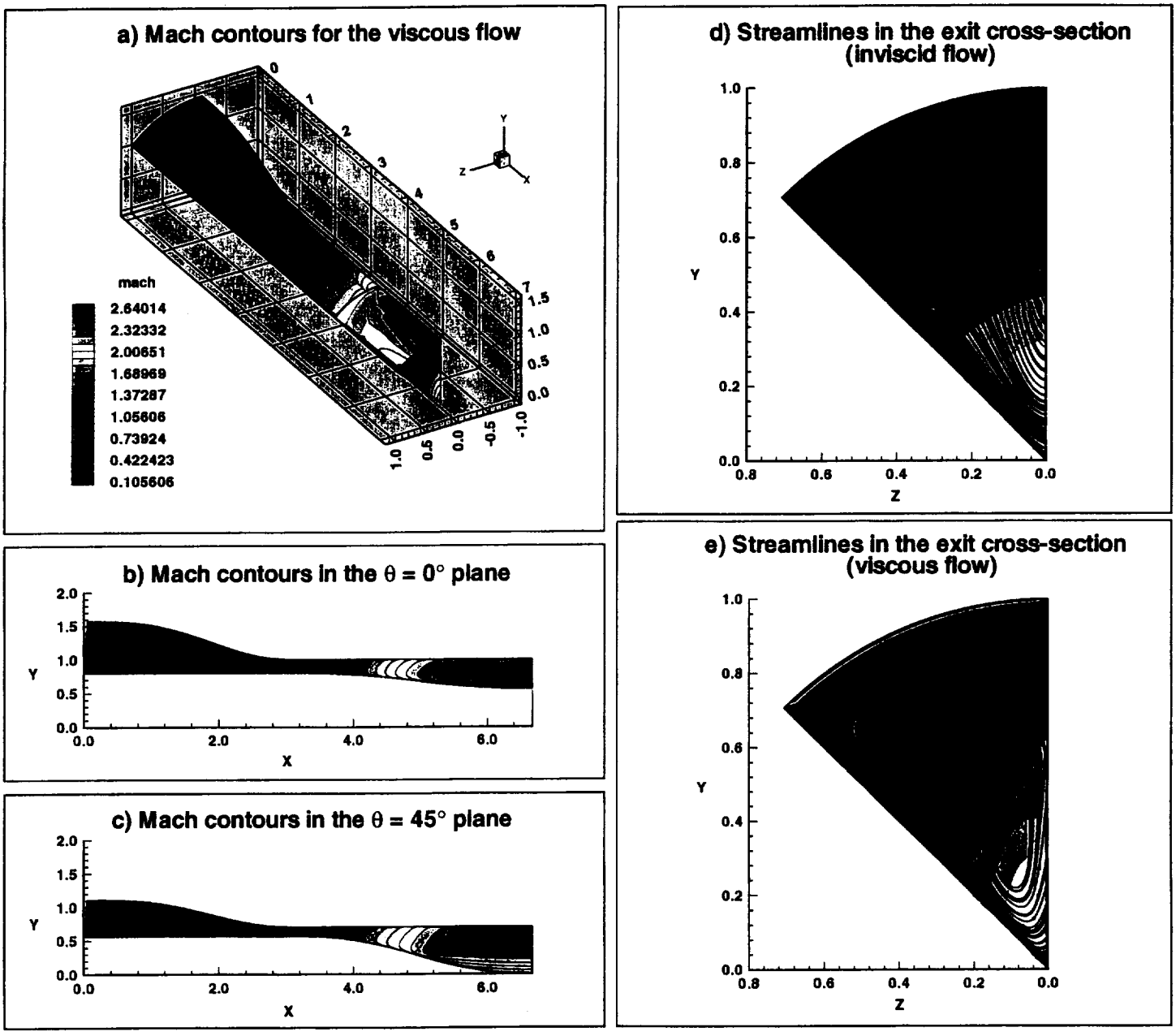

Fig. 18 Mach contours for viscous and inviscid flow simulations (nozzle pressure ratio NPR = $p_o/p_\infty = 2.960$, nozzle temperature ratio NTR = $T_o/T_\infty = 2.817$). **a)** 3-D view of mach contours for a viscous flow within a nozzle with a screwdriver centerbody. **b)** Mach contours in the $\theta = 0°$ plane ($z = 0$). **c)** Mach contours in the $\theta = 45°$ plane. **d)** Mach contours with superimposed streamlines at the nozzle exit (end of the screwdriver centerbody) for an inviscid flow case. **e)** Mach contours with superimposed streamlines at the nozzle exit for a viscous flow case.

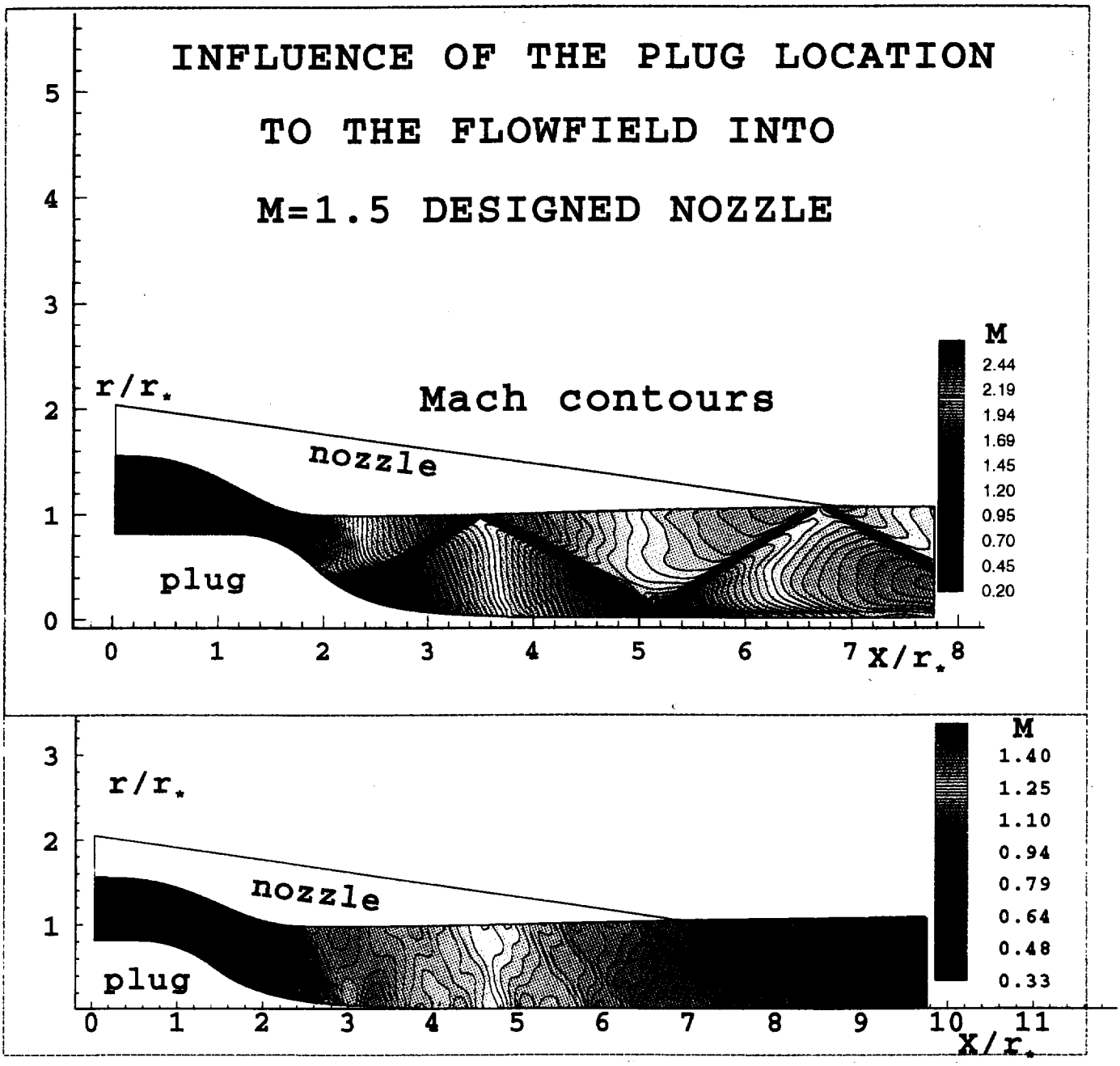

Fig. 19 Influence of axisymmetric centerbody location on the inviscid flowfield within a M=1.5 designed nozzle (nozzle pressure ratio NPR = $p_o/p_\infty = 2.96$). **a)** Mach contours for centerbody located near $x = 2.0$. **b)** Mach contours for centerbody located near $x = 1.0$ (closer to the nozzle inflow).

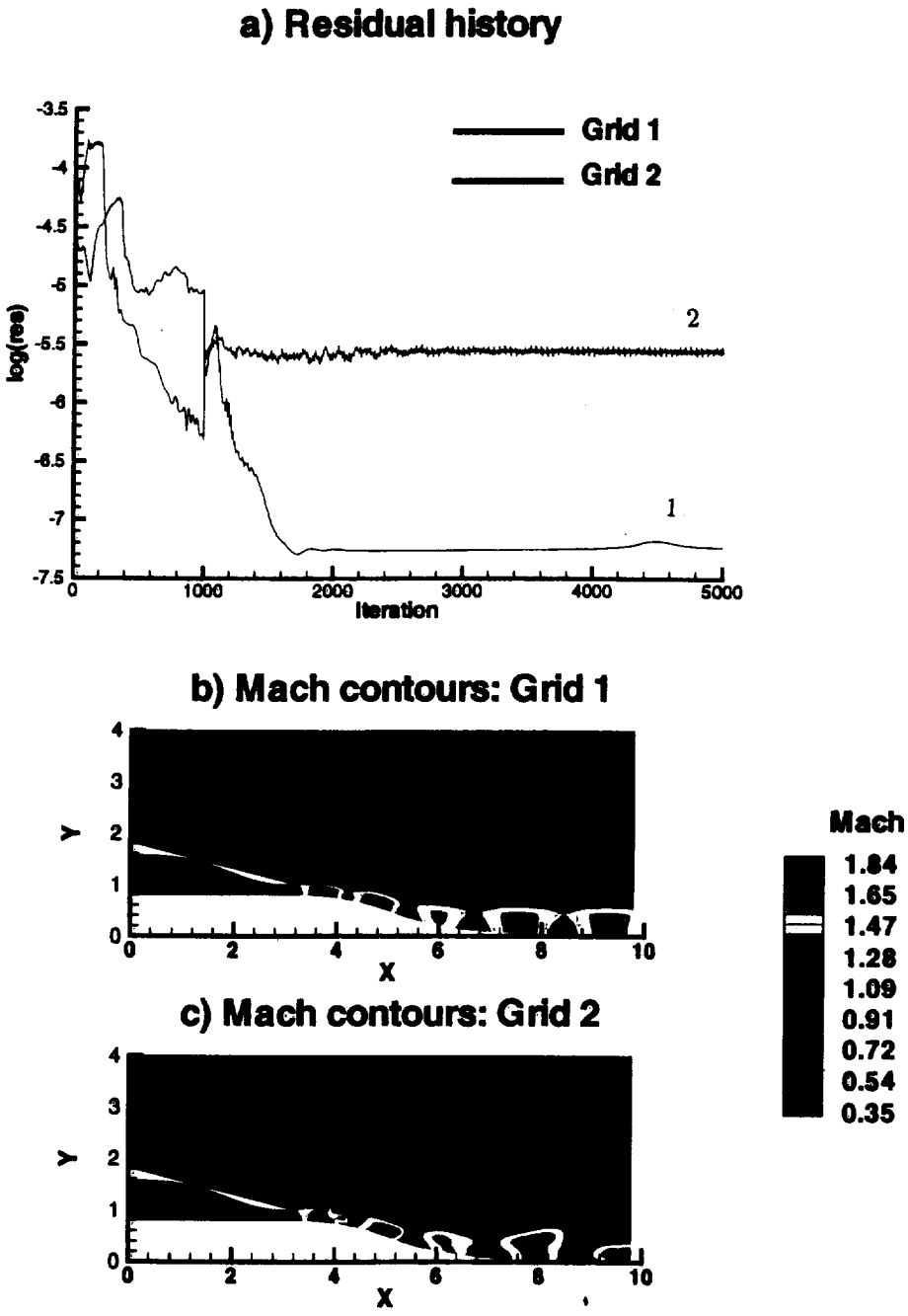

Fig. 20 Residual history and mach contours for an inviscid jet with an axisymmetric centerbody employing two different computational grids (nozzle pressure ratio NPR = $p_o/p_\infty = 3.67$). **a)** Residual history. **b)** Mach contours for grid 1 (coarse grid with dimensions: 162×66). **c)** Mach contours for grid 2 (fine grid with dimensions: 306×154).

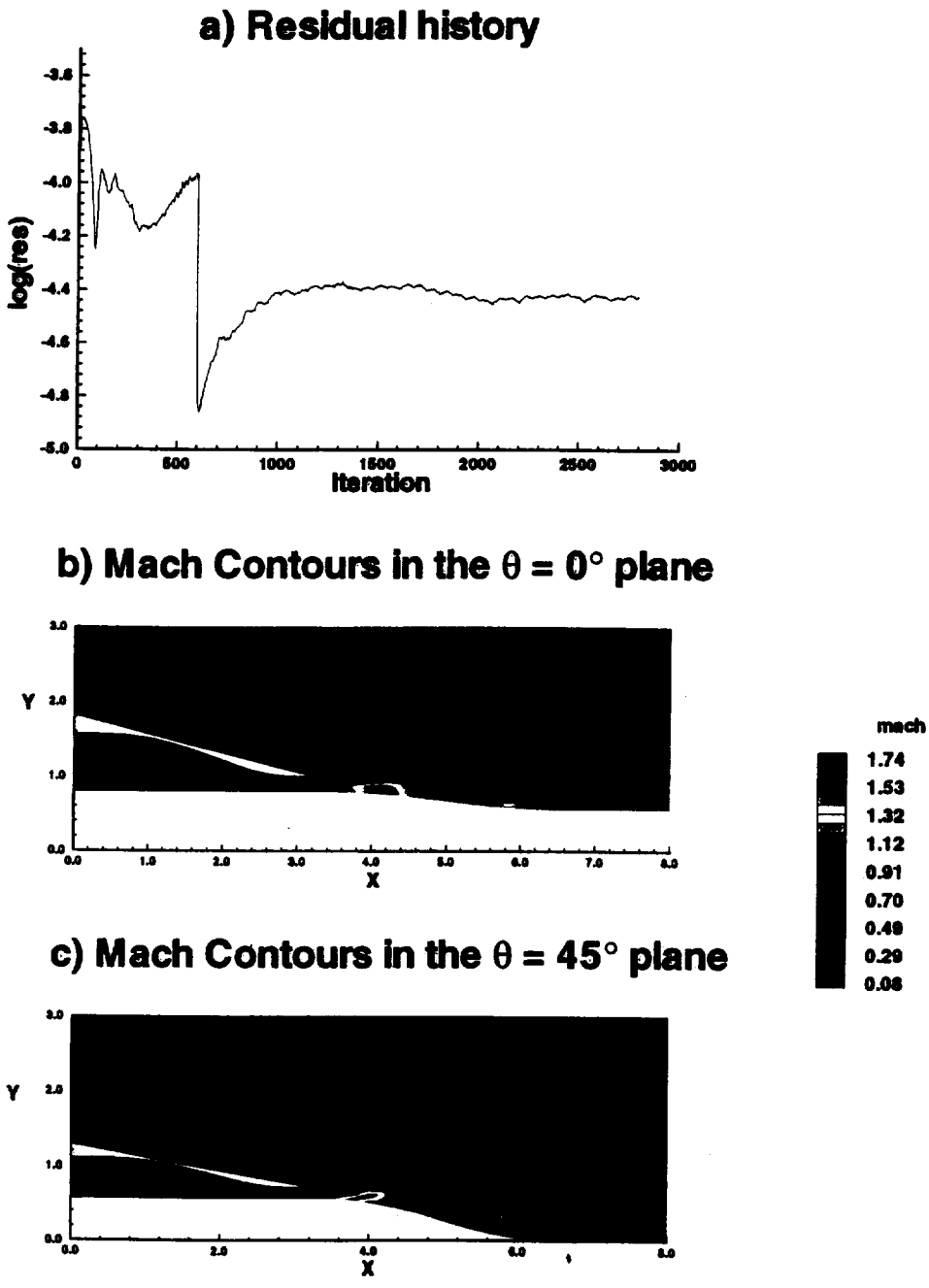

Fig. 21 Residual history and mach contours for an inviscid jet with a screwdriver centerbody (nozzle pressure ratio NPR = $p_o/p_\infty = 2.296$). **a)** Residual history. **b)** Mach contours in the $\theta = 0^o$ plane ($z = 0.0$). **c)** Mach contours in the $\theta = 45^o$ plane.

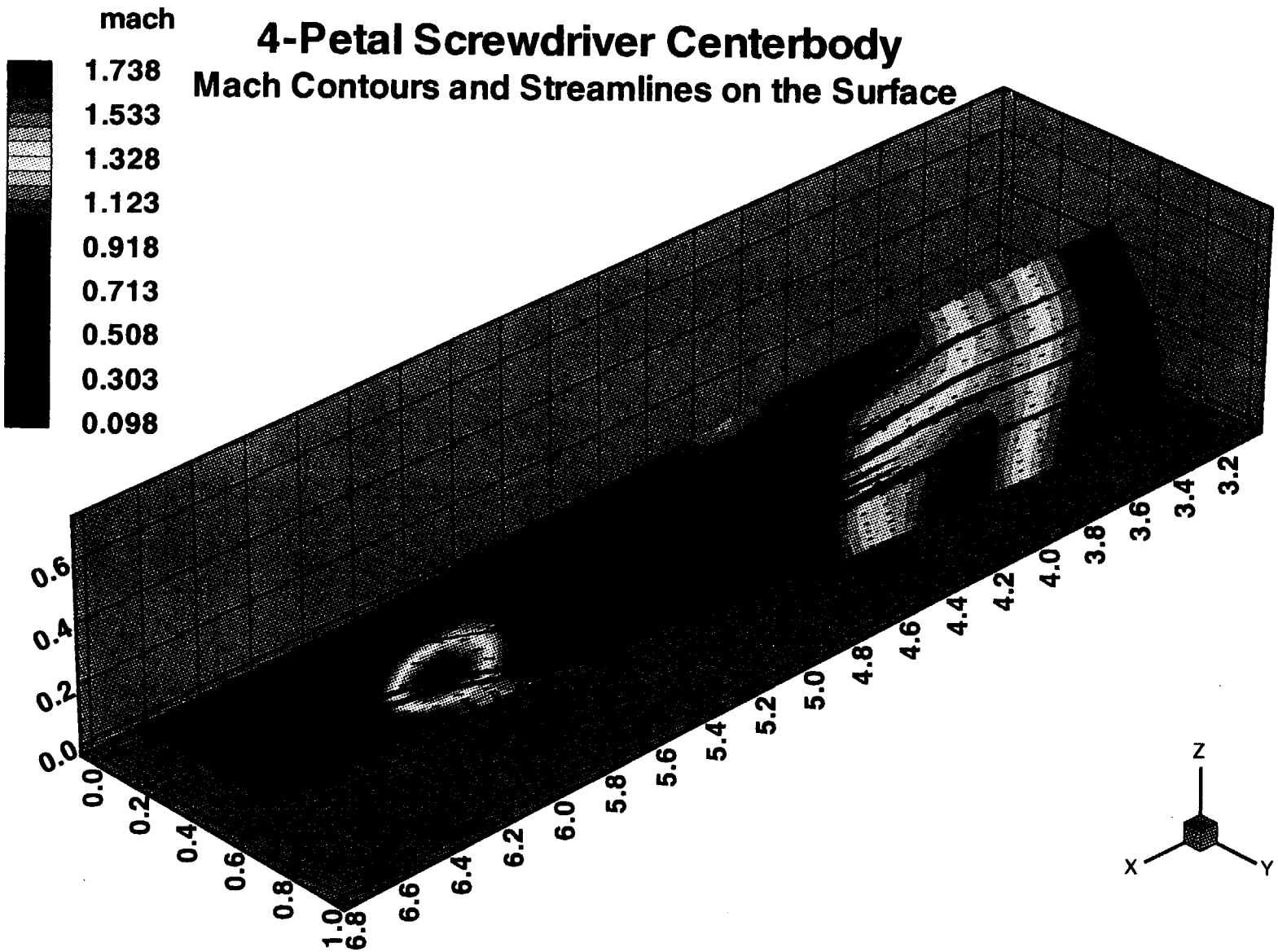

Fig. 22 Mach contours and streamlines on the surface of the screwdriver centerbody of an inviscid jet flow (nozzle pressure ratio NPR = $p_o/p_\infty = 2.296$).

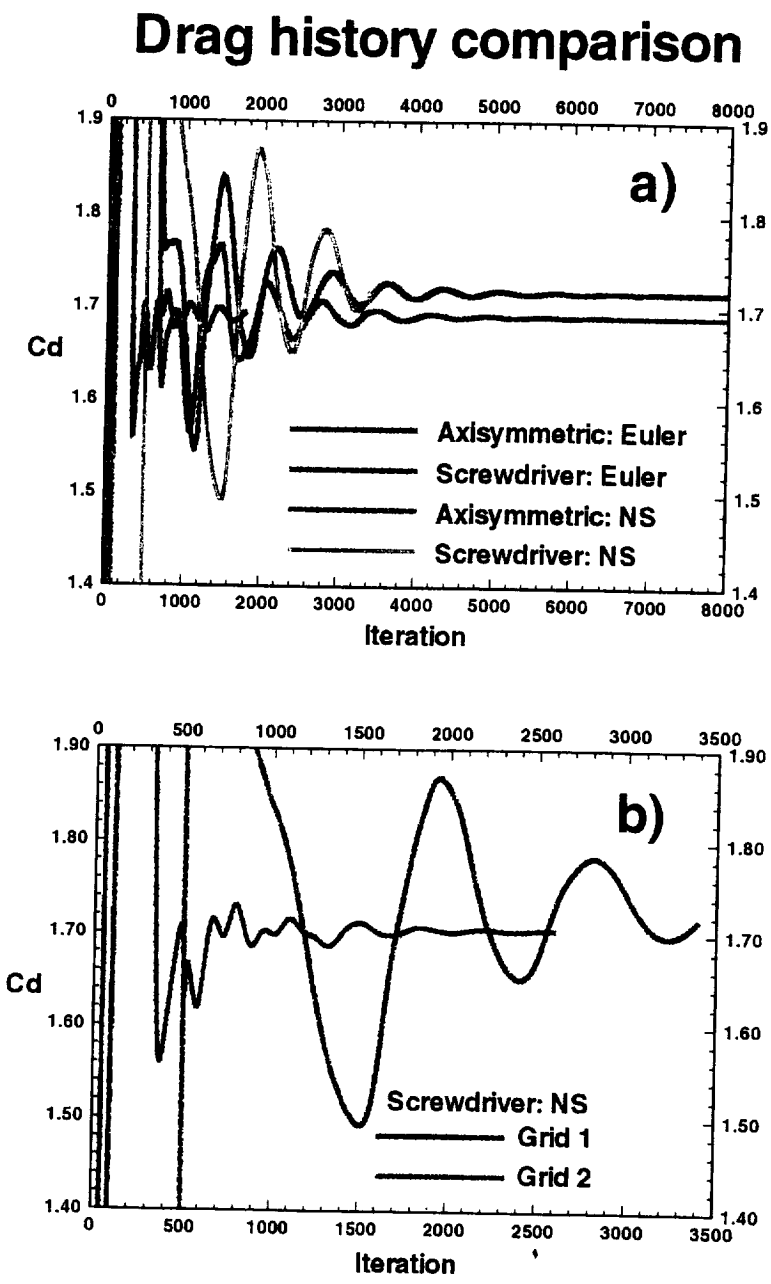

Fig. 23 Drag history for inviscid and viscous nozzle flows with axisymmetric and screwdriver centerbodies (nozzle pressure ratio NPR = $p_o/p_\infty = 2.960$, nozzle temperature ratio NTR = $T_o/T_\infty = 2.817$). **a)** Comparison of several cases showing progression toward a converged value. **b)** Comparison of of viscous nozzle flows with a screwdriver centerbody employing grids with different stretching near the centerbody surface. (Grid 1: grid used in Euler calculations, nearly uniform; Grid 2: grid employing stretching near the wall in attempt to capture some boundary layer effects).